UPPSALA
UNIVERSITET

Digital Comprehensive Summaries of Uppsala Dissertations from the Faculty of Science and Technology 2198

Strategies for finding new magnetic materials

SIMON ROSENQVIST LARSEN

ACTA
UNIVERSITATIS
UPSALIENSIS
UPPSALA
2022

ISSN 1651-6214
ISBN 978-91-513-1617-8
URN urn:nbn:se:uu:diva-486285

Dissertation presented at Uppsala University to be publicly examined in Polhemsalen, Ångströmlaboratoriet, Lägerhyddsvägen 1, Uppsala, Thursday, 24 November 2022 at 09:15 for the degree of Doctor of Philosophy. The examination will be conducted in English. Faculty examiner: Professor John Paul Attfield (Centre for Science at Extreme Conditions, The University of Edinburgh, Edinburgh EH9 3FD, United Kingdom).

Abstract

Larsen, S. R. 2022. Strategies for finding new magnetic materials. *Digital Comprehensive Summaries of Uppsala Dissertations from the Faculty of Science and Technology* 2198. 59 pp. Uppsala: Acta Universitatis Upsaliensis. ISBN 978-91-513-1617-8.

Magnetic materials are indispensable in modern day society. The vast majority of energy generation and conversion involves some kind of magnetic material, and several other applications such as data storage also use them. Despite this there are relatively few types of magnetic materials in use today, which is due to the difficulty of finding new materials that have the necessary properties. In this thesis synthesis of new magnetic materials is performed using a variety oftechniques in an attempt to identify a structured approach to finding crystal structures suited for further development.

Three approaches for developing new magnetic materials were used. Targeted substitutions of Mn was done in $AlCoCrFeMn_xNi$ and $Mn_3Co_{20}B_6$, where Mn provided significant contributions to the magnetic moment, at the cost of stability of the ferromagnetic structures. A new system was identified using theoretical screening, Mn_2Co_3Ge, which was successfully synthesised. Application of the substitution method revealed properties in the system favourable for magnetic refrigeration. New systems were also discovered in synthesis attempts of Mn_2Co_3Ge and Ce-based magnets, but these materials were ferrimagnetic, or canted anti-ferromagnetic, resulting in low magnetisation.

Varying degrees of success were seen in creating magnetic materials with these approaches. Theoretical screening is likely to become an incredibly powerful tool in the future as more understanding of systems is gained. Complementing the theoretical screening method with the newly discovered structures could be a promising avenue for developing new applicable materials. Substitution of elements will remain an extremely powerful tool for tuning properties and by combining it with theoretical screening will likely be key to discovering new applicable magnet systems in the future.

Keywords: Magnetic materials, Materials development, Alloys

Simon Rosenqvist Larsen, Department of Chemistry - Ångström, Inorganic Chemistry, Box 538, Uppsala University, SE-751 21 Uppsala, Sweden.

ISSN 1651-6214
ISBN 978-91-513-1617-8
URN urn:nbn:se:uu:diva-486285 (http://urn.kb.se/resolve?urn=urn:nbn:se:uu:diva-486285)

Dedicated to Annette, Jørn and Theresa.

List of papers

This thesis is based on the following papers, which are referred to in the text by their Roman numerals.

I **S.R. Larsen**, D. Hedlund, H. Stopfel, D. Karlsson, C.K. Christensen, P. Svedlindh, J. Cedervall "Magnetic properties and thermal stability of B2 and bcc phases in AlCoCrFeMn$_x$Ni", *Journal of Alloys and Compounds* **861** (2021) 158450.

II **S.R. Larsen**, D. Hedlund, M. Sahlberg, P. Manuel, P. Svedlindh, E.K. Delczeg-Zcirjak, J. Cedervall "Magnetism and magnetic structure determination of a selected $(Mn,Co)_{23}B_6$-compound" *Journal of Alloys and Compounds* **905** (2022) 164225.

III A. Vishina, D. Hedlund, V. Shtender, E.K. Delczeg-Czirjak, **S.R. Larsen**, O.Y. Vekilova, S. Huang, L. Vitos, P. Svedlindh, M. Sahlberg, O. Eriksson, H.C. Herper "Data-driven design of a new class of rare-earth free permanent magnets", *Acta Materialia* (2021) 116913.

IV **S.R. Larsen**, V. Shtender, D. Hedlund, E.K. Delczeg-Czirjak, P. Beran, J. Cedervall, A. Vishina, T.C. Hansen, H.C. Herper, P. Svedlindh, O. Eriksson, M. Sahlberg "Revealing the Magnetic Structure and Properties of $Mn(Co,Ge)_2$", Accepted for publication in Inorganic Chemistry 2022.

V D. Hedlund, **S.R. Larsen**, M. Sahlberg, P. Svedlindh, V. Shtender "Influence of Mn/Co ratio on the magnetic properties of hexagonal $Mn(Co,Ge)_2$ phase", Submitted.

VI V. Shtender, **S.R. Larsen**, M. Sahlberg "Variants of the X-phase in the Mn-Co-Ge system", *Acta Crystallographica. Section C* **77** (2021) 176-180.

VII V. Shtender, D. Hedlund, **S.R. Larsen**, P. Svedlindh, M. Sahlberg "Structural and magnetic properties of new members of the 3:29 phase from the Ce–Fe–Mn system and 1:11 from the Ce–Co–Mn", *Journal of Alloys and Compounds* **855** (2021) 157435.

Reprints were made with permission from the publishers.

Disclaimer: Parts of this thesis are based on my licentiate thesis entitled *Harnessing the Magnetic Potential of Manganese in Selected Cubic Compounds* (Uppsala University 2021).

Contributions of the author to the papers:

I Planned the study. Synthesised the samples, carried out X-ray diffraction and calorimetric measurements and analysis of those results. Wrote part of the manuscript with input from other authors.

II Took part in planning the study. Synthesised the sample, participated in X-ray and neutron scattering measurements. Participated in analysis and discussion of results. Wrote part of the manuscript with other authors.

III Took part in sample synthesis and X-ray diffraction measurements. Participated in analysis and discussion of results. Wrote part of the manuscript with other authors.

IV Planned the study. Participated in neutron diffraction measurement and in the analysis and discussion of results. Wrote the manuscript with input from other authors.

V Took part in planning the study, participated in the analysis and discussion of the results and provided feedback on the manuscript.

VI Synthesised samples and participated in the analysis and discussion of the results. Wrote part of the manuscript with other authors.

VII Participated in sample synthesis and X-ray diffraction measurements. Participated in analysis and discussion of results.

The author has also contributed to the following papers which are not included in the thesis:

1. **S.R. Larsen**, M. Hansteen, B. Pacakova, K. Theodor, T. Arnold, A.R. Rennie, G. Helgesen, K.D. Knudsen, H.N. Bordallo, J.O. Fossum, L.P. Cavalcanti "Sample cell for studying liquid interfaces with an in situ electric field using X-ray reflectivity and application to clay particles at oil-oil interfaces", *Journal of Synchrotron Radiation* **25** (2018) 915-917.

2. L.P. Aldridge, **S.R. Larsen**, H.N. Bordallo "Octave program for fitting quasi-elastic neutron scattering data", *Physica B: Condensed Matter* **561** (2019) 75-78.

3. **S.R. Larsen**, L. Michels, É.C. dos Santos, M.C. Berg, W.P. Gates, L.P. Aldridge, T. Seydel, J. Ollivier, M.T.F. Telling, J.O. Fossum, H.N. Bordallo "Physicochemical characterisation of fluorohectorite: Water dynamics and nanocarrier properties", *Microporous and Mesoporous Materials* **306** (2020) 110512.

Contents

1. Introduction

"Once a young boy he set out
Upon the road to fame and fortune
Full of hope for all looks bright in daylight
But the young boy he must learn
That road is twisted and turns
And dangerous to travel after midnight"
-Wuthering Heights

1.1 Magnetic materials

Materials have always played an important role for humanity. They were originally used for finding food and water, but were later developed for other uses. So important were these materials that time periods, known as ages, have been named after the most important material in use. These include the stone age, bronze, and iron ages with some referring to the modern age as the silicon age. A unique material was discovered hundreds of years B.C. which had the property of being able to attract iron. This was the lodestone, and its ability to attract iron and other lodestones is what we now know as magnetism. This was probably the first encounter humanity had with a magnetised material [1, 2].

While lodestones saw application as compasses and showed their novel ability to attract many iron-based materials, the understanding of them and the underlying physics did not change much. It was first when H.C. Ørsted noticed a compass needle reacting to an electrical current that the connection to electricity was established. This connection is so deep that these days it is called electromagnetism, and indeed, both electricity and magnetism have their origin in the movement of electrons, with magnetism being seen as a relativistic effect of these movements. Some of the strongest magnetic fields are produced by these movements of charges in the so called electromagnets, which are used in everything from scrapyard magnets to windmills and powerful research equipment.

In the magnets not relying on an electrical current it is instead the quantum mechanical spins that are the source of the field, with the electrons being the main contributor. As the magnetic moment is determined by the spin, overall magnetic interactions are only seen for unpaired electrons since the opposing spin of a pairing electron cancels out the magnetic moment. This cancellation of moment leads to what is called diamagnetism, where an outside applied

magnetic field changes the movement of the electrons resulting in an opposing field being generated. Unpaired electron moments often point in random directions in space, but can be aligned using an external field, which results in the material being known as a paramagnet. The unpaired electron moments can also find it energetically favourable to align to each other. This can happen in a variety of ways, of which the most well-known is ferromagnetism. Ferromagnetism is what we commonly associate with the common refrigerator magnet and here the moments align parallel pointing in the same direction, as seen in figure 1.1 a). In some cases antiparallel alignment is more favourable leading to the cancellation of the magnetisation despite the alignment, this is called anti-ferromagnetism and is sketched in figure 1.1 b). When the same does not result in the perfect cancellation of the moments as shown in figure 1.1 c), it is instead a ferrimagnet which has similar but weaker properties as the ferromagnet [3]. More complicated alignments are also possible such as the canted anti-ferromagnet (figure 1.1 d)), where the anti-ferromagnetic moments tilt along a specific axis, resulting in a small net magnetisation. The incommensurate configuration (figure 1.1 e)) is a family of complicated configurations, and is typified by a long range order which, while periodic cannot be described by a finite amount of unit cells. Finally there are certain cases where anti-ferromagnetic interactions will compete with each-other in the system, which cannot be easily resolved leading to magnetic frustration (figure 1.1 f)).

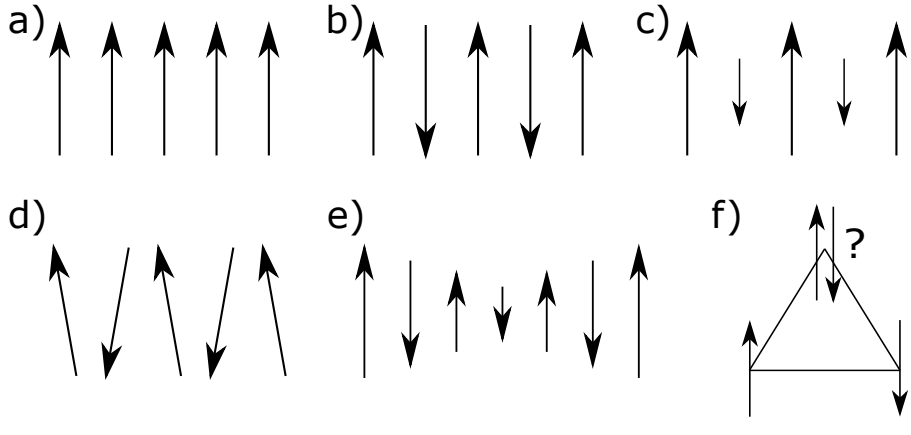

Figure 1.1. The ordering of spins in the case of a) a ferromagnet, b) an anti-ferromagnet, c) a ferrimagnet, d) a canted anti-ferromagnet, e) an incommensurate structure and f) a magnetically frustrated system.

These days the close relation of electricity and magnetism has resulted in magnetic materials playing an incredibly important role in society. Their use in generators means that they are necessary for providing the majority of electricity used. They are also used in the electronics themselves, to store data on hard drives and in speakers, for instance [4]. More recently, there has also

been interest in using the magnetocaloric effect of magnets as a new method of refrigeration, which would significantly reduce the amount of electricity used for cooling [4]. Other industries simply want the ability of magnets to attract other magnetic elements. With such a wide range of applications, it is desirable to have an equally wide range of magnets with properties to cover all these applications. Despite this, only a few applied magnetic systems exist, these being the rare-earth free Alnico and ferrites, and the rare-earth based SmCo and the famed NdFeB. The SmCo and NdFeB can together cover most of the current applications, but they are very expensive to make, and the rare-earth elements needed for their creation have since 2011 been seen as a contested strategic resource [5]. On the other hand, the cheaper and plentiful rare-earth free magnets are not powerful enough, or are needed in such amounts that implementation is impossible, that they cannot substitute for the rare-earths in all applications. Finding new systems that could fill in some for some of these applications is thus highly desirable [5].

1.1.1 Magnetic properties

There are several properties that determine which applications a magnetic material can be used for. The magnetisation, as has been mentioned, is perhaps the simplest to understand as it denotes the concentration of the magnetic moments in the material. The larger the magnetisation, the stronger the magnet is. When an external magnetic field is applied on a ferro- or ferrimagnetic material the spins align and magnetisation increases, but it will reach a practical limit called the saturation magnetisation (M_{sat}) where it only increases extremely slowly. The behaviour of the magnetisation when the applied field is removed is used to classify it into one of two groups. The first group are the hard magnetic materials, which are able to maintain their magnetisation without an external field and are used as permanent magnets. The soft magnetic materials constitute the other group which are easy to magnetise, but quickly lose it without the field present, and are used in applications that require this quick switch, like transformers. A comparison of these two types can be seen in figure 1.2. The magnetisation can also be lost due to thermal fluctuations destroying the order of the magnetic moments and causing the material to become paramagnetic. The thermal transition from the ferro or ferrimagnetic state to the paramagnetic state is called the Curie temperature (T_C) and is another of the main properties investigated when trying to find applicable magnets. The relatively low T_C of 583 K for NdFeB magnets is one of the reasons that it cannot be used in all applications. If the material instead orders anti-ferromagnetically and experiences a transition to the paramagnetic state, it is called the Néel transition (T_N).

To determine whether a material is likely to be a hard or soft magnetic material, the magnetic anisotropy is often considered. Magnetic anisotropy is a

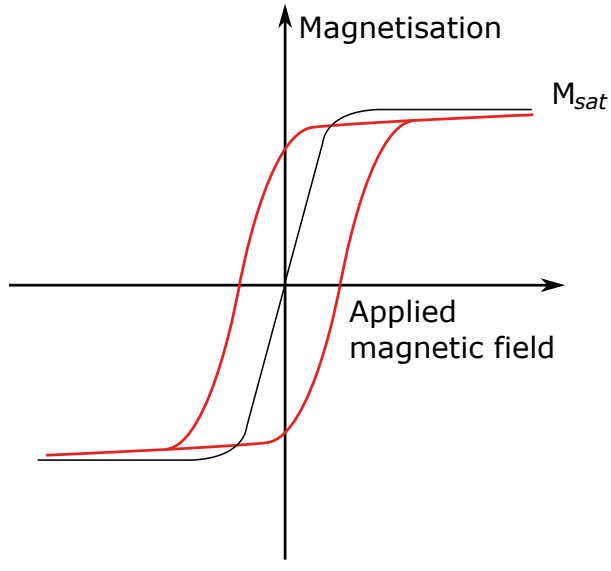

Figure 1.2. A pictoral representation of hysteresis curves of hard (red) and soft (black) magnetic materials. The soft magnetic material rapidly reaches saturation when a field is applied, but loses it as the field is removed. The hard magnetic material retains some magnetisation, and requires a field applied in the opposite direction (or passing T_C) to reach zero magnetisation.

measure of directional preference of the magnetic moments. In soft magnetic systems, there is often little to no anisotropy while it is a necessity and determines the direction of the magnetisation in hard magnets. There are many contributors to anisotropy, but the easiest to control is the magnetocrystalline anisotropy, which arises from the crystal structure of the system. In cubic systems, such as with the lodestone, the high symmetry results in many favourable magnetisation directions, and little magnetocrystalline anisotropy. The material instead has to rely on other anisotropic features, such as the physical shape of the crystal, or grains, to maintain the magnetisation in a specific direction. Generally there is a clear preferred direction that the moments align along, called the easy axis, and an axis which is very difficult to align along, called the hard axis. The difference in energy required to align the moments along the easy and hard axis is called the magnetic anisotropy energy (MAE), and can be used to give an estimate of whether magnetic material will be hard or soft.

1.1.2 Finding magnetic systems

Considering the vast majority of the elements in the periodic table are either diamagnetic or paramagnetic, the search for magnetic materials is focussed on a select few elements. Fe, Co and Ni are the main elements, as they are

the only elements which naturally are ferromagnetic above room temperature. The most well-known magnetic element, Fe, has a single pair of spins in the d orbital with the four others being unpaired. Co and Ni, the other most common elements, have two-three pairs of spins leaving fewer unpaired spins, resulting in a lower magnetic moment. The other element near Fe, Mn, has in its groundstate a half-filled d orbital, resulting in five unpaired spins. A comparison of the spins of Mn and Ni can be seen in figure 1.3 with Fe and Co containing one and two more electrons than Mn respectively. Despite the large number of unpaired spins, Mn is not ferromagnetic at room temperature and even becomes anti-ferromagnetic at lower temperatures [6]. The complex interactions between electrons are the reason for this, but by increasing the interatomic distance between the Mn atoms the unfavourable interactions can be avoided [7–10]. These elements are currently the main building blocks when creating applicable magnetic materials.

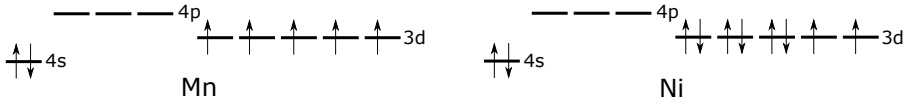

Figure 1.3. A simplified representation of the electron configuration for isolated Mn and Ni atoms, the elements surrounding the stronger magnetic elements Fe and Co.

Historically, magnetic materials have mainly been found through two approaches. The first of these was the substitution of elements resulting in a magnetic alloy, which provided the earliest magnetic steels. The second is the targeted development of a new system, as was seen for NdFeB magnets, which were discovered by clever selection of elements motivated by a desire to lower the cost of SmCo magnets. Accidental discoveries and luck also played a role, such as in the very early days of the development of MnAl [11, 12].

Access to computers with large computational power has prompted new methods for predicting and finding materials with desired properties, and magnetic materials are no exception. Several approaches exist, but most attempts focus on using Fe, Co, Ni or Mn in a specific crystal structure and calculating the expected properties. For permanent magnets the properties estimated this way are the magnetic moment of the atoms in the unit cell, the T_C and the anisotropy. The anisotropy is sometimes simply accounted for by ensuring that the crystal structure is not cubic.

1.2 Systems studied

The classical approach to develop magnetic materials, as well as the computationally aided method, were applied in this thesis to find magnetic materials. The targeted substitution method was applied as the main technique in two cases, the $AlCoCrFeMn_xNi$ system, and the $Mn_3Co_{20}B_6$ system. The com-

putational method was applied to find Mn_2Co_3Ge before the substitutional method was applied again. Finally, while trying the direct approach by synthesising a specific crystal structure, some unexpected discoveries were made, especially of note are the $Ce_3(Fe_{0.638}Mn_{0.362})_{29}$ and $CeCo_8Mn_3$ systems. An introduction to the materials follows.

1.2.1 AlCoCrFeMnNi

AlCoCrFeMnNi is considered by some to be a high-entropy alloy (HEA). HEAs are a class of alloys discovered in 2004 [13–15] which distinguish themselves from conventional alloys by not consisting of a single major element. A single definition for HEAs has not been agreed upon yet, but they are in most cases described as consisting of five or more elements in a single phase solid solution. Many systems labelled as HEAs do not conform to this description, however, leading to other descriptive names such as Multi-Principal Element Alloys (MPEA) and Complex Concentrated Alloys (CCA). Due to the involvement of many elements in significant quantities, high-entropy alloys have been investigated for a wide range of applications, such as additive manufacturing [16], hydrogen storage [17], catalysis [18] and more importantly, within magnetism [19]. The sheer tunability of their properties continuously attracts research in an effort to expand the library of materials available for applications [20, 21].

HEAs get their name from the high configurational entropy of mixing that arises due to the number of elements in the system. Alloy systems minimize the Gibbs free energy of formation by forming the most energetically favourable structures. The Gibbs free energy of the solid solution system is described as:

$$\Delta G^{SS} = \Delta H^{SS} - T\Delta S^{SS} \tag{1.1}$$

Where H^{SS} is the enthalpy, T is the temperature and S^{SS} is the entropy of mixing. As the enthalpies for a solid solution and an intermetallic compound are rather similar, it is the entropy that has a large degree of influence over whether the solid solution forms or not. The entropy for the solid solution is given as:

$$\Delta S^{SS} = -R\sum c_n ln(c_n) \tag{1.2}$$

with R being the gas constant and c_n being the atomic concentration of element n. As mentioned, the number of elements in high concentrations has a sizeable impact on the entropy contribution and thereby the Gibbs free energy. As such, the solid solution is said to be entropy stabilised. However, the solid solution still competes with intermetallic phases energetically. If the Gibbs free energy of the HEAs is higher than that of any intermetallic phases ($G^{SS} >$

G^{IM}) then it will not form the solid solution phase. For HEAs this entropy value is often defined to be $S^{SS} > 1.61R$ [22, 23].

As intermetallic structures often energetically compete with HEAs, it is not uncommon for them to appear in the HEA systems. This is often exemplified with the appearance of some degree of longer range ordering in the sublattices, typical of the intermetallic B2 (CsCl-type) structure. This ordering is often as result of the addition of elements with a larger atomic size compared to the rest of the alloy constituents. In figure 1.4 an intermetallic system, a HEA and the pseudo-ordered HEA are presented.

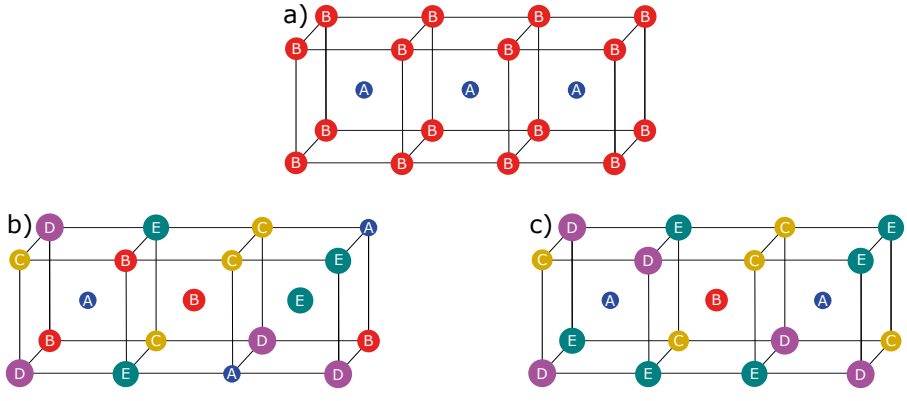

Figure 1.4. The crystal structures for a) an ordered two-element compound, b) a HEA with random occupancies on the sites and c) a pseudo-ordered HEA showing preferential occupancies.

In order to describe the formation of solid solution HEAs, the Hume-Rothery rules were extended as follows [24, 25]:

1. The difference of the atom sizes, Δ, should be smaller than 6.6%
2. The ratio between $T\Delta S$ and ΔH should be larger than 1.1
3. The enthalpy of mixing should be between -20 and 5 kJ/mol

The Hume-Rothery rules were originally intended for use in binary or ternary systems and adapting it for use with HEAs required several modifications. The many elements in a true HEA should have the same probability of occupying a given site, and all elements thus need to be considered solute. The reduction of the original Hume-Rothery size difference of 15% to 6.6% ensure that all elements can substitute one another. The introduction of the enthalpy of mixing is used as an indicator of compatibility of the elements. As there are many different interactions possible, this needs to be constrained. A too negative a value would result in more favourable intermetallic compounds being formed rather than the solid solution, while a too positive value would have the mixing being energetically unfavourable, preventing it from mixing. The ratio of $T\Delta S$

and ΔH being above 1.1 is the entropy stabilising part of the HEAs. A large entropy lowers the free energy, hindering ordering and segregation thereby promoting the solid solution over the intermetallics phases.

The Valence Electron Concentration (VEC) also has a significant impact on the HEA system, especially in regards to what lattice type it crystallizes in, promoting the tunability of the system. Generally a higher VEC will result in cubic close packed (ccp) type structures being preferred while a lower VEC will result in body centred cubic (bcc) type structures [26]. The low VEC of Al is one of the main reasons it is used to stabilise the bcc configurations, which are important for a variety of properties in HEAs [27]. Examples of favourable properties of bcc phases are the hardness of $CuCoNiCrAl_xFe$ [13] and the predicted magnetic properties of AlCoCrFeNi and CoCrFeGaNi [28]. In fact, many of the HEA systems that have attracted attention for the combination of their soft magnetic properties and durability crystallise in the bcc configuration. This is due to the magnetic moments having a tendency to align more easily in the bcc configuration than the ccp configuration. This results in a larger saturation magnetisation, a property often optimised in soft magnets. The increase in saturation magnetisation is often large enough that the inclusion of non-magnetic elements to stabilise the bcc system is seen as favourable as noted for Al, Ga and Sn in AlCoFeMnNi, CoFeMnNiGa and CoFeMnNiSn [29].

1.2.2 $Mn_3Co_{20}B_6$

The $Cr_{23}C_6$ structure has been known since the 1930s and is a structure often seen in steels [30]. The large cubic structure with space group $Fm\bar{3}m$ is shown in figure 1.5. The number of crystallographic sites available and the possibility of intermixing on some of these sites result in a large degree of freedom over the composition of the alloy. This has led to the family of structures often being described as $M_{23}Z_6$ [31] or $M_{23\text{-x}}M'_xZ_6$ [32]. Here M is most often a transition metal and M' is likely also a transition metal but has also been known to include lighter metals and rare earth elements. Finally there is Z which contains the smaller interstitial site elements such as C, B or P. Ordered variants of the ternary system exist. In $Cr_{21}W_2C_6$ [33] the 8c site is occupied solely by W, while the $Mg_3Ni_{20}B_6$ structure has 4a and 8c sites being exclusively occupied by the M' element [34]. A comparison of site occupancy of the systems can be found in table 1.1.

The magnetic properties of the system $Al_3M_{20}B_6$, an ordered structure, were investigated for Co and Ni where Fe was substituted into certain positions. The magnetic properties ranged from a high magnetisation and Curie temperature for Fe which decreased with the additions of Co, to becoming completely paramagnetic when large amounts of Ni were present [35]. The compounds $Mn_3Ni_{20}P_6$ and $Mn_3Pd_{20}P_6$ exhibit some magnetic properties car-

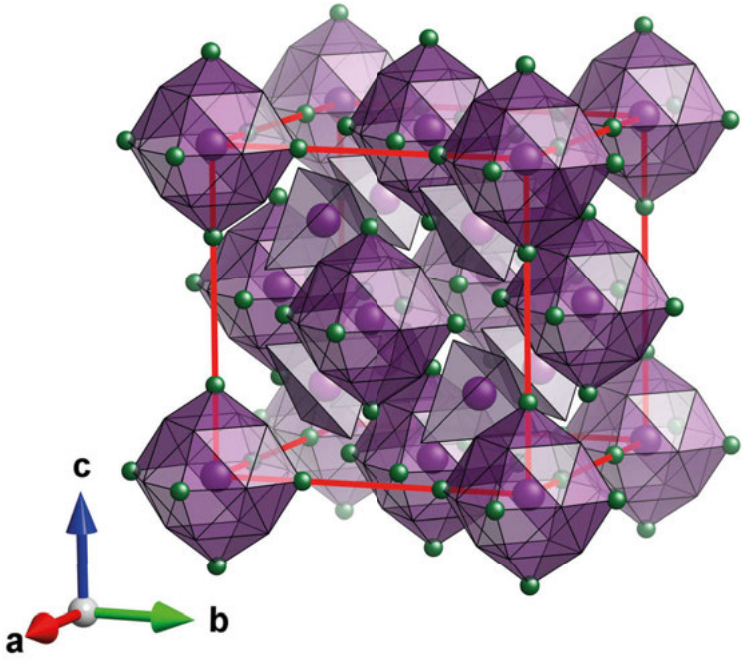

Figure 1.5. The crystallographic structure of the $Cr_{23}C_6$-type structure. C in green and Cr is shown in purple, with the open corners of the polyhedra which coordinate the 4*a* and *8c* sites, also being Cr.

ried solely by the presence of Mn [36, 37] with Ni and Pd acting paramagnetically. That Mn in these cases contributes to the magnetic properties to such a degree, is due to the 4*a* and 8*c* sites which host the Mn atoms. Though both $Mn_3Ni_{20}P_6$ and $Mn_3Pd_{20}P_6$ exhibit magnetic order determined by the moment of Mn there were differences in the ordering itself. While $Mn_3Pd_{20}P_6$ has a ferromagnetic structure at lower temperatures, $Mn_3Ni_{20}P_6$ has independent anti-ferromagnetic ordering of the Mn sites. This is attributed to the sizeable difference in Mn-Mn distances of 0.38–0.61 Å more in $Mn_3Pd_{20}P_6$ compared to in $Mn_3Ni_{20}P_6$ [36, 37].

Table 1.1. *Relations between $Cr_{23}C_6$ and its related ordered structures.*

Atom	Wyckoff position	$Cr_{23}C_6$	$Cr_{21}W_2C_6$	$Mg_3Ni_{20}B_6$
Z	24*e*	C	C	B
M1	48*h*	Cr	Cr	Ni
M2	32*f*	Cr	Cr	Ni
M3	8*c*	Cr	W	Mg
M4	4*a*	Cr	Cr	Mg

1.2.3 Mn_2Co_3Ge

Mn_2Co_3Ge was first discovered in the 1960s when two versions of the crystal structure were reported, the $MgZn_2$-type and the ordered Mg_2Cu_3Si-type [38]. The $MgZn_2$ structure type is one of the three Laves phase structure types, the others being $MgCu_2$ and $MgNi_2$. These three structures are all closely related, differing only in how a four layer unit is stacked in the system [39, 40].

The Laves phases are very common structure types and there are examples of Laves phases created by elements throughout almost the entire periodic table. This naturally results in a wide range of potential properties for which they are investigated, such as hydrogen storage [41] and wear resistance [42]. Their presence is sometimes seen as detrimental as their brittle nature can severely reduce the strength of materials such as steels [43, 44], prompting much research into controlling when they appear in materials.

The $MgZn_2$ structure type [45] discussed here crystallises in space group $P6_3/mmc$ with the atoms entering into the three crystallographic sites, $2a$, $4f$ and $6h$. The $4f$ site is typically occupied exclusively by the more electropositive element, with the $2a$ and $6h$ being occupied by the other elements, and are typically capable of a large degree of intermixing. In a few rare cases the $2a$ and $6h$ sites are occupied exclusively by specific elements, resulting in the structure type of Mg_2Cu_3Si [46]. The low number of atoms in the unit cell, and the large degree of ordering make $MgZn_2$ and especially Mg_2Cu_3Si attractive systems for computational studies. The ordered Mg_2Cu_3Si structure is visualised in figure 1.6.

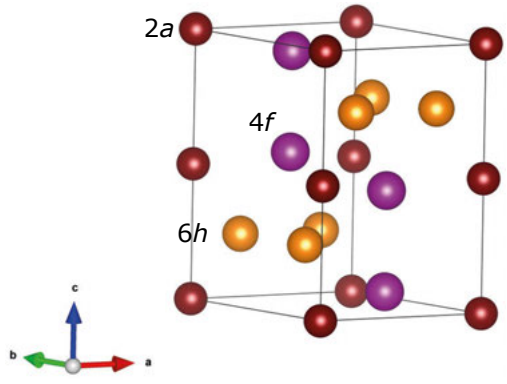

Figure 1.6. The crystallographic structure of Mg_2Cu_3Si, with Si on the red $2a$ positions, Mg on the purple $4f$ positions and Cu on the yellow $6h$ positions.

1.2.4 Ce-transition metal based structures

Much like the original work done to find cheap rare-earth based magnets, which gave rise to NdFeB, there are attempts to use the even lighter and

cheaper rare-earth elements. This has mostly focussed on Ce, with particular interest being given to the structures even richer in transition metal than the NdFeB 2:14 phase. $ThMn_{12}$ and Th_2Ni_{17} are two well-known structure types that manage this.

In the $ThMn_{12}$ structure [47], space group $I4/mmm$, the rare-earth element occupies the corner and body-centred 2*a* site and the transition metals occupy the other sites of 8*f*, 8*i* and 8*j*. Though it has potential for a high density of magnetic moments in the structure, there is only one example of a binary structure of a rare-earth and Fe, $SmFe_{12}$ [48]. A third element is usually needed to help stabilise the structure [49]. The $ThMn_{12}$ structure is related to the $CaCu_5$-type, by partial replacement of rare-earth atoms with transition metal atoms [50].

The Th_2Ni_{17} structure [51] is a hexagonal structure which is related to the $CaCu_5$ structure in a similar way as the $ThMn_{12}$-type phase. Th_2Ni_{17} is often called the high-temperature phase, as at lower temperatures, and for systems based on the lighter rare-earths, the rhombohedral structure Th_2Zn_{17} often forms instead [52, 53]. The 1:12 and rhomobohedral 2:17 phases combine in some cases, resulting in a new structure with the stoichiometry 3:29. This structure is made of alternate stacking of 1:12 and 2:17 layers in a 1:1 ratio, resulting in a monoclinic structure with space group $P2_1/c$ where the rare-earth element occupies the 2*a* and a single 4*e* site, and the transition metal the 2*d* site and the 14 remaining 4*e* sites [54, 55].

An unrelated structure that can form in certain rare-earth alloys is $CeMn_6Ni_5$ [56]. This structure type has the space group $P4/mbm$ with the rare-earth element in the 2*a* position and the transition metal atoms in 2*c*, 4*g*, 8*k* and 8*j* positions. The ordered variant structure YNi_9In_2 [57] divides the transition metal sites so that the 4*g* site is occupied exclusively by one element, and the 2*c*, 8*k* and 8*j* sites by the other.

2. Scope of the thesis

Due to magnets having a vital role in making our society function, having a large library of materials to choose from for various applications is useful. The current magnet market is however dominated by only a few kinds of magnets. These can be divided into two main groups: the powerful but expensive rare-earth magnets NdFeB and SmCo, and the weak but cheap rare-earth free magnets ferrites and Alnico. Between these two groups there is a gap in properties and price, shown in figure 2.1, which has yet to be filled. Any application which requires a material with properties within this gap are forced to use the more expensive rare-earth magnets instead. As a result of this, much research into magnet materials are these days focussed on finding a way to cover this property gap.

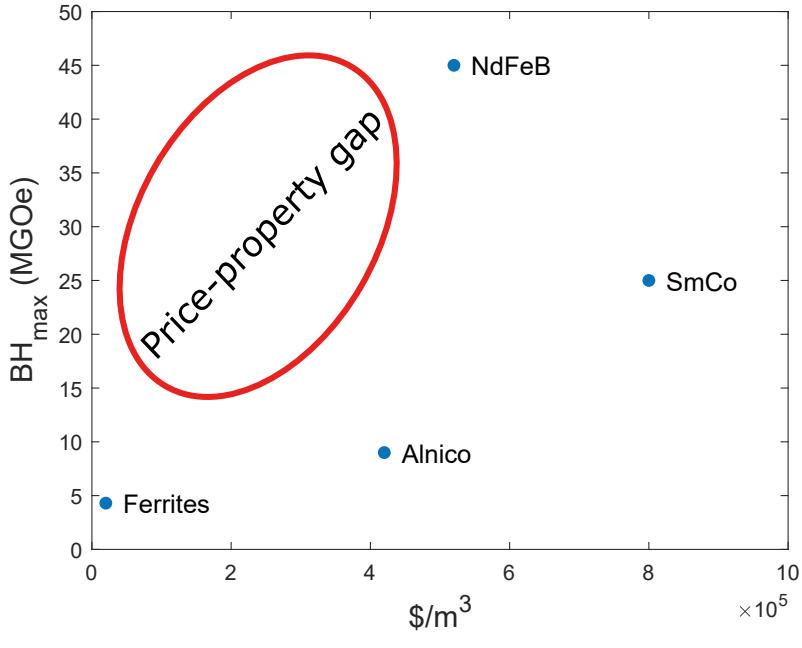

Figure 2.1. The maximum energy product and price per volume of common applied magnets, with the gap in performance and price emphasised with an ellipse. Data taken from [58].

Magnetic materials created for specific applications are may be improved in a variety of ways. These are mainly focussed on improving the microstruc-

ture, by aligning grains or providing a proper environment to ensure permanent magnetisation. Though the microstructure is one of the most important features, the underlying crystal structures of the system set the baseline for many of the properties it exhibits. This is often seen as the main area where magnetic material development is focussed, for without the appropriate crystal structures there is no microstructure to improve. For materials that are to be used in typical environments there are two main methods which are applied when trying to improve the crystal structure of the system. These methods are by either substituting one element in the crystal structure for another, or by using a different crystal structure. Both of these methods have their difficulties. With substitutions, there are limitations on the amount of the element which can be substituted into the structure used. On the other hand, attempting to find new stable structures with favourable properties is a difficult and very time consuming task. The many competing physical interactions between atoms make them difficult to predict, and the direct experimental method of discovering and isolating new structures is laborious.

This thesis focusses on development of magnetic materials on the crystal structure scale. The aim is to evaluate strategies for creating new magnetic materials, including targeted elemental substitutions, theoretical screening and direct experimental methods. This is mainly done through the synthesis and structure- and property characterisation of the systems presented. In these systems manganese will play a major role, as it is either a main component of the compounds, or the element added in an effort to improve magnetic properties.

3. Methods

"Make them glow!
Make them burn!
Mining, carrying, forging, crafting, smelting of the ores"
-Wind Rose

3.1 Synthesis techniques

3.1.1 Arc melting

Arc melting utilises an electrical arc between a tungsten rod and a water-cooled copper hearth to heat metals. Due to the large voltage difference when the arc is struck, the gas is turned into a conducting plasma, which allows for rapid heating to high temperatures. All high entropy alloy samples were synthesised by melting the constituting elements in an argon atmosphere. This atmosphere served both as the source of the current carrying the plasma and as a protective gas. Furthermore, a titanium "getter" was melted for three minutes to interact with any remnant oxygen present in the chamber. Homogeneity was promoted by flipping and the re-melting the sample five times. An illustration of this technique can be seen in figure 3.1 a).

3.1.2 Induction melting

Sending a high-frequency alternating current through a coil generates a rapidly alternating magnetic field. When a conducting material is present in the magnetic field, eddy currents are generated in the material. These eddy currents disperse throughout the material as heat, heating up the material. When the material becomes molten the magnetic field causes it to move instead, this results in good mixing of the elements in the melt. Furthermore, as the material is only heated up to the temperature required to melt it, elemental losses using induction melting are low, though some volatilisation can still occur. As such the induction furnace, illustrated in figure 3.1 b), is an excellent method for synthesising alloys.

For laboratory purposes arc-melting is often preferred as the first synthesis method as it can quickly be used to test ideas for samples. The higher temperatures and the quicker cooling of the sample help to reduce segregation and also allows the formation of different microstructures than accessible with annealing. Induction melting is preferred when alloys with a narrow stoichiometric ranges are synthesised, as fewer losses and better mixing result in a more homogeneous alloy.

3.1.3 Powder sintering

A common technique for synthesising samples from powder is sintering. Sintering utilises heating or pressure induced diffusion to form a solid material from powders without melting the elements. To avoid interaction with elements in the air, sintering is usually done in vacuum or using a protective inert gas, such as Ar. Samples are therefore sealed inside steel or Ta tubes, or in glass ampoules to avoid interaction with the local atmosphere. Depending on the materials involved in the synthesis it might be necessary to employ a crucible to avoid interactions with the tube or ampoule. Due to this synthesis technique being reliant on diffusion, it often requires a significant amount of time to complete. This permits a rather large degree of control over the heating program which can be used to target certain temperature regions of stability. Rapid cooling from the higher temperatures using quenching can help lock these structures in place, permitting synthesis of a wide range of structures. An outline of powder sintering in a pit furnace is illustrated in figure 3.1 c).

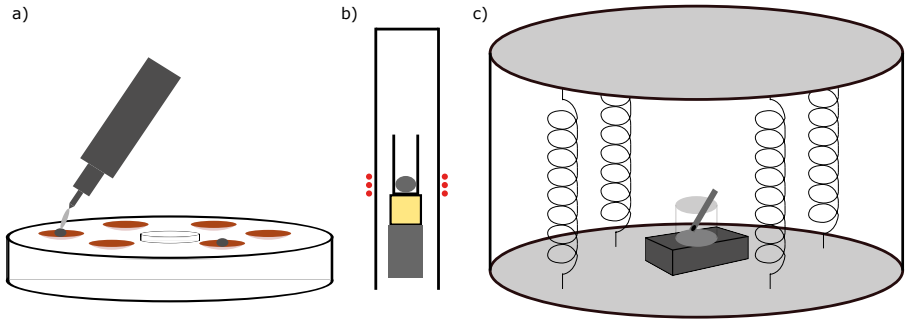

Figure 3.1. Illustrations of the equipment used for the sample synthesis. a) an arc-furnace for arc-melting, b) a induction furnace, and c) a pit-furnace for sintering.

3.2 Diffraction

Diffraction is one of the most well-established experimental techniques when it comes to investigating the characteristics of solid matter. It was originally discovered using X-rays, which have wavelengths comparable to the interatomic distances in crystals. This permits coherent scattering from parallel crystal planes in the material. The elastically scattered waves can interfere constructively or destructively with one another leading to a distinct pattern dependent on the crystal structure. For constructive interference to occur the waves must, in addition to being scattered elastically, have the same path-length. The law that describes how this is fulfilled is called Bragg's Law:

$$n\lambda = 2dsin(\theta) \tag{3.1}$$

In order to remain in phase, the wavelength λ must remain the same or be multiplied by full integers n. The wave must travel an additional distance both incoming and outgoing equal to twice the distance between the crystal planes, d multiplied with sine of the incident angle, θ. The relationship between these variables can be seen in figure 3.2. Bragg's Law provides information about the distance between planes and thereby the unit cell parameters, but it is not sufficient to give an idea of the atomic positions in the structure. For this information the intensity, which is the measurable quantity, has to be considered. The intensity is generally described by equation 3.2 [59].

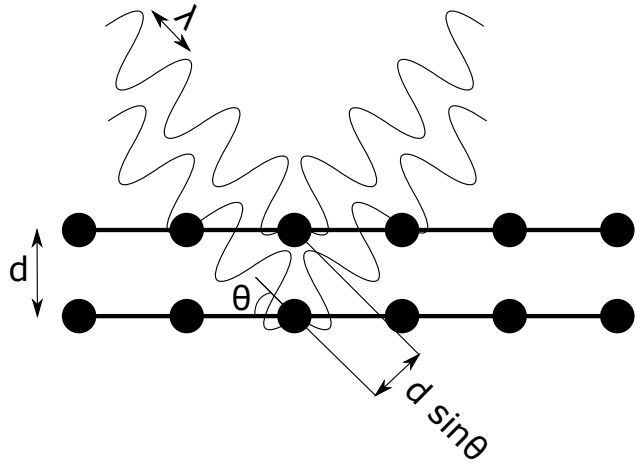

Figure 3.2. Elastically scattered radiation. In order to achieve the same pathlength the lower wave must travel an additional $dsin(\theta)$ to and from the plane, resulting in $2dsin(\theta)$.

$$I_{hkl} = K \cdot p_{hkl} \cdot L_\theta \cdot P_\theta \cdot A_\theta \cdot T_{hkl} \cdot E_{hkl} \cdot |F_{hkl}|^2 \tag{3.2}$$

Where K is the scale factor relating to the amount of phase, measurement time and flux of the incident radiation, p_{hkl} is the reflection multiplicity, L_θ, P_θ and A_θ are correction factors for geometry, polarisation and absorption of the beam, T_{hkl} is the preferred orientation factor and E_{hkl} is the extinction correction, which in powders is negligible. Finally F_{hkl} is the structure form factor which relates the crystal structure to the intensity and is defined in equation 3.3.

$$F_{hkl} = \sum_{j=1}^{n} N_j f_j e^{2\pi i \cdot (hx_j + ky_j + lz_j)} T_j \tag{3.3}$$

Here N_j is the contribution from occupancy, f_j is the atomic scattering factor, $2\pi i \cdot (hx_j + yk_j + zl_j)$ is the phase angle of the atom j at the coordinates x_j, y_j, z_j and finally T_j is the temperature factor. As X-rays scatter off the

electrons the atomic scattering factor becomes proportional to the number of electrons in the atom. The observable quantity is intensity, but equation 3.2 shows that it is proportional to F_{hkl}^2. The squaring of the complex number F_{hkl} converts it to a real number, which results in the loss of the information of the phase. Due to the phase containing information about the electron distribution in the structure it is of vital importance. Without it the phases have to be guessed or extracted from the data by other means. This is known as the phase problem.

To gain information about the structure the Rietveld refinement method [60] implemented in the software FullProf [61] was used. This method uses a basic model as input and refines the parameters of it to best agree with the data. The Rietveld method considers the intensity contributions from the structure form factor, correction factors and other contributions relating to the sample or the instrument. Several parameters are used to evaluate how well the model agrees with the data. This begins with R_p, seen in equation 3.4 which gives an indication of the difference between the observed data points, $y_i(obs)$, and the point calculated from the model, $y_i(calc)$. A large background can however unfavourably skew this calculation, and often a modified version of the parameter is used called R_{wp}, shown in equation 3.5. R_{wp} uses a weighing parameter, w_i, which increases the importance of the higher intensity data points, thereby ensuring that matching of actual reflections is more important than the background.

$$R_p = \sum_i |y_i(obs) - y_i(calc)| / \sum_i y_i(obs) \tag{3.4}$$

$$R_{wp} = \sqrt{\sum_i w_i [y_i(obs) - y_i(calc)]^2 / \sum_i w_i [y_i(obs)]^2} \tag{3.5}$$

The data quality is also evaluated when comparing models. This is done using R_{exp}, seen in equation 3.6, which gives an indication of the best possible R_{wp} that can be expected from the data. The difference in the amount of data points, N, and refined parameters, P, ensures that the model is not overdetermined. How comparatively close the model comes to the expected best case scenario is evaluated with χ^2, presented in equation 3.7.

$$R_{exp} = \sqrt{(N-P) / \sum_i^N w_i y_i(obs)^2} \tag{3.6}$$

$$\chi^2 = (R_{wp}/R_{exp})^2 \tag{3.7}$$

The XRD measurements used in this thesis were conducted on two in-house setups and one at a synchrotron source. The in-house experiments were conducted on a Bruker D8 with Lynx-Eye position-sensitive detector using monochromatised CuKα_1 radiation and on a Bruker D8 Advance diffractometer with a Lynx-EyeXE position-sensitive detector using conventional CuKα

radiation. The synchrotron measurements were conducted on the beamline P02.1 at the German Electron Synchrotron (DESY) in Hamburg, Germany using $\lambda = 0.20710$ Å and a Perkin Elmer XRD1621 area detector. Temperature measurements conducted in-situ used a Jensen-type gas cell [62] mounted with a quartz glass capillary and under Ar atmosphere. Kanthal wire wrapped around the capillary supplied the heating of the sample up to 900 °C.

3.2.1 Neutron scattering

Since X-rays interact with the electron cloud their scattering power scales with the number of electrons present. As a result of this it is hard to locate lighter elements such as H, Li and B in a crystal structure where heavier elements are also present. X-rays also have difficulties in discerning between electronically similar elements such as Cr, Mn, Fe, Co and Ni, given that there are only minor differences in the scattering factor due to small difference between the number of electrons present.

It is also possible to perform scattering on a material using neutrons. Neutrons primarily interact with the nucleus of an atom and as such the scattering length, seen in figure 3.3, does not scale in the same way as it does with X-rays. As such the atomic scattering factor contribution is altered in the structure factor (equation 3.3), with the X-ray scattering factor f_j being replaced by the neutron scattering factor b_j.

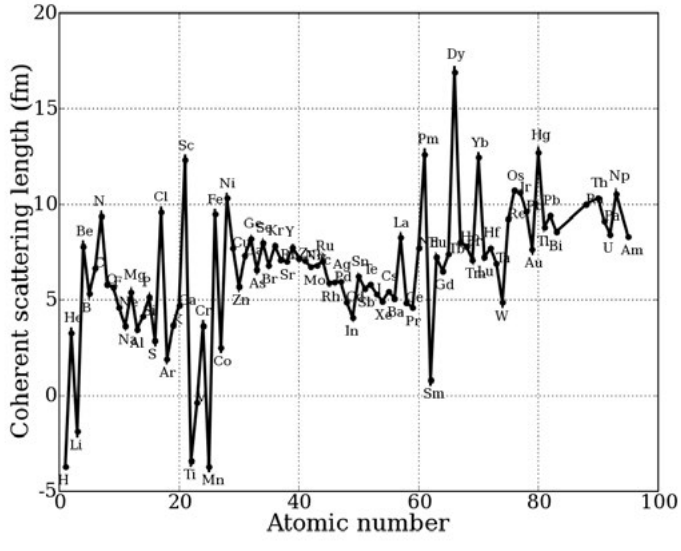

Figure 3.3. Neutron scattering lengths for the naturally occurring elements. [63]

Though neutron scattering is an excellent complement to X-rays, careful consideration must be given to the samples being measured. One such reason is due to how neutrons mainly interact with the nucleus instead of the electron cloud. This interaction can result in absorption of the neutron rather than scattering and has some dependence on the isotope of the element. Boron is one such example where the ^{10}B isotope has an absorption cross section of 3835 b, b being 10^{-28} m^2, compared to the absorption cross section of ^{11}B of 0.0055 b. To avoid loss of signal in B samples they are therefore often synthesised using isotopically pure ^{11}B.

While neutrons mainly interact with the nucleus of an element they also have a magnetic moment of their own. Due to this magnetic moment and the fact that it does not have an electrical field the neutron can interact with the ordered spins of electrons in a material. A diffraction pattern can thus arise from the interaction with the ordered spins. This diffraction can provide additional intensity to existing Bragg peaks or new Bragg peaks can arise due to the ordering occurring over several crystallographic unit cells. As the magnetic contribution arises from interactions with electrons, the magnetic scattering shows some similarities to X-ray scattering, with the form factor decreasing at larger Q.

Neutron Powder Diffraction (NPD) experiments done at D1b, at ILL in Grenoble, France required the sample to be mounted in 8 mm diameter vanadium cylinder and measured in the temperature range of 1.8 K to 396 K using a wavelength of λ = 2.52 Å. For the NPD experiments carried out using the WISH instrument at the ISIS facility in Didcot, United Kingdom, the sample was also mounted in a cylindrical vanadium container but scanned in the temperature range of 6 K to 700 K.

3.3 Magnetic characterisation

The magnetisation of a material is dependent on temperature and the applied magnetic field. Thus when investigating the magnetic properties of the samples both the temperature and the magnetic field have to be considered while measuring magnetisation. As such the magnetisation is often measured as a function of one parameter while the other is kept constant. A superconducting quantum interference device (SQUID) uses the quantised nature of the magnetic flux in a closed loop of superconducting material and the Josephson effect, which describes tunnelling of superconducting electron pairs across a barrier, to measure the magnetic moment of a sample. A vibrating sample magnetometer (VSM) measures the magnetic properties by vibrating the sample at a particular frequency, inducing a voltage in nearby stationary pick-up coils. A Quantum Design MPMS XL and a LakeShore VSM equipped with a furnace measured the magnetic data presented in this thesis.

3.4 Electronic structure calculations

Predicting the properties of a material can be a great asset to find the limits of its applications. The foundation for these predictions is the Schrödinger equation, which needs to be solved for the system. Precious few exact solutions for the Schrödinger equation of physical systems exist, with the limit currently being at one electron model systems. Instead properties can be estimated by replacing the wavefunctions with electron densities, as done within Density Functional Theory (DFT) calculations [64, 65]. In papers II and IV the magnetic structures observed were modelled using the Kohn-Sham one-electron equations as implemented in the Spin-Polarised Relativistic Korringa-Kohn-Rostoker (SPR-KKR) code [66].

The prediction of magnetic materials for paper III was a stepwise process. Database searches were conducted identifying materials with a unit cell with 40 or less atoms in it, consisting of two different 3*d* elements with no restriction on the total amount of elements. The magnetic moments were then calculated within DFT using RSPt electron structure code [67, 68] and assuming a ferromagnetic configuration for all systems. If the material had above 0.4 T saturation magnetisation, it passed to the next stage where cubic systems were discarded. The ground state configuration was then calculated and the materials which had already had the magnetic properties reported were discarded. If a material survived to this point its MAE was calculated, and if it was deemed acceptable a final estimation of the Curie temperature was done.

4. Results and discussion

"Rise my brothers we are blessed by steel
Arm yourselves the truth shall be revealed"
-Ensiferum

4.1 Targeted substitutions

Initial attempts at finding new magnetic materials focussed on the simple substitution of elements into known materials. In this case Mn was sought to be incorporated into the crystal structures of the HEA AlCoCrFeNi and a larger cubic compound $Mn_3Co_{20}B_6$ with the intent of improving the saturation magnetisation of the system.

4.1.1 Enhancing high-entropy alloys

AlCoCrFeNi was the first system where substitutions with Mn to improve the magnetic properties was attempted. Due to the nature of HEAs of being an alloy stabilised by the many elements already in place made this seem like an ideal first test case. In paper I, five alloys of $AlCoCrFeMn_xNi$ with 0, 4, 8, 12 and 16 at.% Mn were synthesised to see how the magnetic properties were affected. As seen in table 4.1 which was derived from XRD patterns e.g. figure 4.1, the structure did not seem to be influenced much by the addition of Mn. This in spite of the main stabiliser of the bcc phase, Al [27], being diluted by the other elements and Mn, which often forms ccp phases. Though Mn did seem to have a slight preference for the B2 phase, it still distributed itself fairly evenly throughout the alloy, thereby avoiding the unfavorable Mn-Mn interactions.

Table 4.1. *Refined unit cell parameters and phase fractions for the $AlCoCrFeMn_xNi$ samples. Standard errors are given in the parentheses.*

	a [Å]		Phase fraction [wt.%]	
x	B2	bcc	B2	bcc
0	2.8768(2)	2.8638(2)	49(1)	51(1)
0.04	2.8752(2)	2.8665(2)	45(2)	55(2)
0.08	2.8816(2)	2.8697(2)	40(2)	60(2)
0.12	2.8886(3)	2.8729(2)	26(1)	74(2)
0.16	2.8865(2)	2.8732(2)	57(1)	43(1)

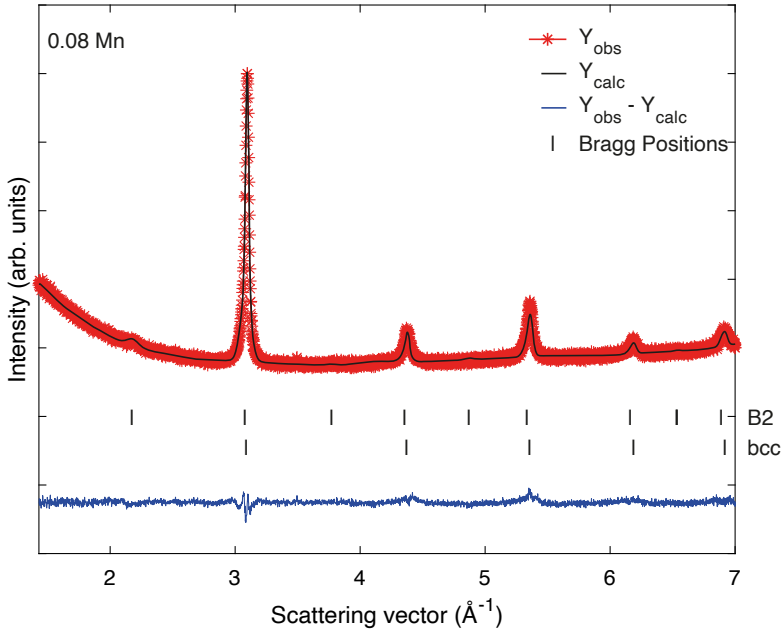

Figure 4.1. XRD pattern for the $AlCoCrFeMn_{0.08}Ni$ sample. The data is presented as a black line, while the calculated profile is seen in red. The Bragg reflections for these are seen below the data as marked lines, the B2 phase on top with the bcc phase below. The blue line shows the difference between model and data. Other samples with different Mn content exhibit the same two phases of the ordered B2 and disordered bcc.

With successful incorporation of Mn into the alloy in all cases, the resulting influence on the magnetic properties was studied. As seen in Figure 4.2 the saturation magnetisation generally increased in a linear fashion from 0.44 T with no Mn to 0.74 T with an equimolar amount of Mn. As this HEA and Alnico magnets both share the feature of a spinodally separated two-phased system with AlNi and Fe rich regions, they were compared. The saturation magnetisation was on a comparable level to early Alnico magnets, before much development had gone into the microstructure, or in-field annealing was considered.

Additions of Mn lowered the onset temperature for decomposition of the alloy into an ccp type phase, which had been predicted to have worse magnetic properties, and the non-magnetic σ-phase. The appearance of these phases is also reflected in the magnetic measurements seen in Figure 4.3, which shows the earlier drop off of the magnetisation. In this case Mn enhances the creation of the non-magnetic phase at the cost of the slightly magnetic fcc phase. As Cr is the main reason why the non-magnetic phase is formed, it could potentially be removed from the alloy or replaced with more stabilising Al for better

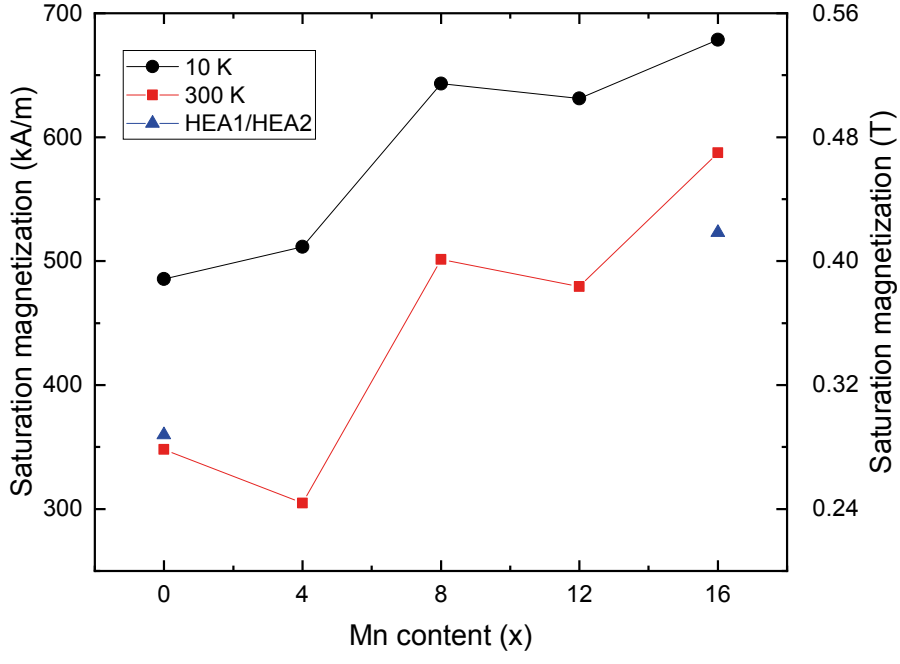

Figure 4.2. Saturation magnetisation as a function of Mn content at various temperatures. HEA1/HEA2 were single-phased gas atomised versions of the alloys added for comparison.

results. Nevertheless, the stability is comparable to the Alnico magnets, and adding Mn could be a potential method for increasing the magnetisation.

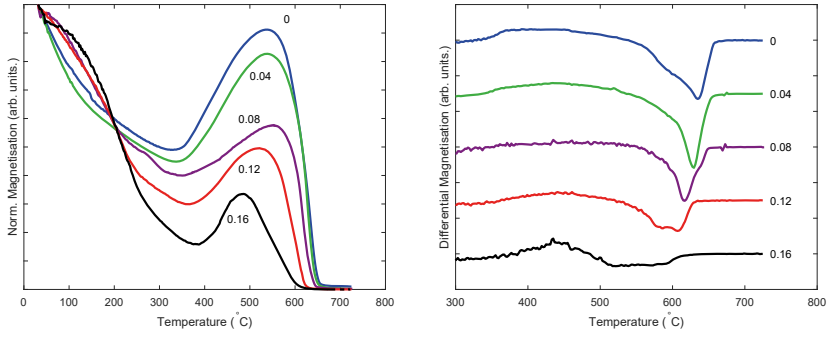

Figure 4.3. Magnetisation curves for heated samples with the corresponding differential curve. The differential curves have been offset for better readability.

4.1.2 The large cubic system $Mn_3Co_{20}B_6$

Instead of randomly dispersing Mn atoms throughout an entire structure and hoping for improved properties, the targeting of specific atomic positions in a structure was attempted. This was done in paper II, where it was attempted to have Mn occupy the 4*a* and 8*c* positions of a Co-based $Cr_{23}C_6$ structure. These crystallographic positions have been reported to be able to host specific atoms, giving rise to the structures of $Cr_{21}W_2C_6$ and $Mg_3Ni_{20}B_6$. Neutron diffraction was conducted to confirm the location of Mn in the structure and investigate the contribution of Mn to the overall magnetic moment of the system. The distribution of Mn in the structure was established by model refinements of the data, seen in figure 4.4. The values extracted, which are seen in table 4.2 indicated that while Mn did have a preference for the intended sites, it did not exclusively occupy it and it also entered into other sites in the structure.

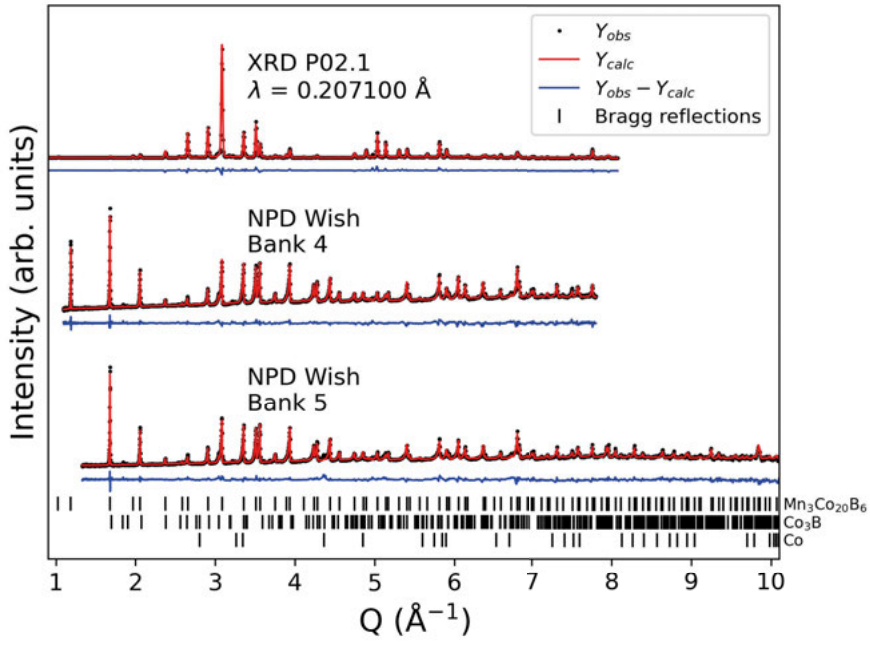

Figure 4.4. Refinements of crystallographic structure using combined synchrotron XRD and NPD data at 700 K.

The magnetic structure was investigated next, using the established paramagnetic structure as a basis. While several potential magnetic structure models could fit the data they all showed features of ferrimagnetism due to Mn moments. The magnetic space group chosen to represent the system was $I4/mm'm'$, and the extracted magnetic moments can be seen in table 4.3, while a visualisation of the structure is displayed in figure 4.5. The Mn-rich 8*c* site provided the largest local magnetic moments in the structure of 2.22 μ_B com-

Table 4.2. *Occupancies and atomic position extracted from combined refinement of XRD and NPD data at 700 K for $Mn_{4.7}Co_{18.3}B_6$. The standard error is shown in the parenthesis. The unit cell parameter was found to be a = 10.5873(3) Å.*

Atom	Wyckoff position	x	y	z	Occupancy
B	24*e*	0.2743(3)	0	0	1
Co1	48*h*	0	0.1701(4)	0.1701(4)	0.878(5)
Mn1	48*h*	0	0.1701(4)	0.1701(4)	0.122(5)
Co2	32*f*	0.3828(4)	0.3828(4)	0.3828(4)	0.878(5)
Mn2	32*f*	0.3828(4)	0.3828(4)	0.3828(4)	0.122(5)
Mn3	8*c*	0.25	0.25	0.25	0.800(4)
Co3	8*c*	0.25	0.25	0.25	0.200(4)
Mn4	4*a*	0	0	0	0.507(3)
Co4	4*a*	0	0	0	0.493(3)

pared to the largest moment of Co-rich sites, 1.04 μ_B. However, the other Mn-rich site, 4*a*, provided the only anti-ferromagnetically aligned moments. Despite the large amount of Mn present on this site, these moments were rather small comparatively, and in an effort to understand the reason for this DFT calculations were employed.

The calculations revealed that the small anti-ferromagnetic moment on the 4*a* site was due to a combination of the negative Mn moments and strong positive Co moments. Furthermore, the calculations also indicated that there were strong ferromagnetic couplings between the Mn on the 4*a* site and Mn on the high multiplicity sites surrounding it. This also contributed to the low anti-ferromagnetic moment on this site, though it was hampered by the tendency for these same high multiplicity sites to couple anti-ferromagnetically to one-another. Calculation of the total energy of the system indicated that despite the large distance between the Mn atoms in a completely ordered system, the 4*a* moments would still anti-align to the other moments. The Mn atoms on the 48*h* would actually contribute to stabilising a ferromagnetic structure over a ferrimagnetic one, if they could be separated well enough from other Mn atoms on this site.

Table 4.3. *Magnetic moment of the dominant element at the positions extracted from refinements of the 6 K data. The standard error is shown in the parenthesis. a = 10.5022(3) Å.*

Atom	Wyckoff position	x	y	z	Magnetic moment (μ_B)
Co1(1)	48*h*	0	0.1695(4)	0.1695(4)	0.90(3)
Co1(2)	48*h*	0.1695(4)	0.1695(4)	0	1.04(5)
Co2	32*f*	0.3826(1)	0.3826(1)	0.3826(1)	0.36(3)
Mn3	8*c*	0.25	0.25	0.25	2.22(6)
Mn4	4*a*	0	0	0	-0.48(5)

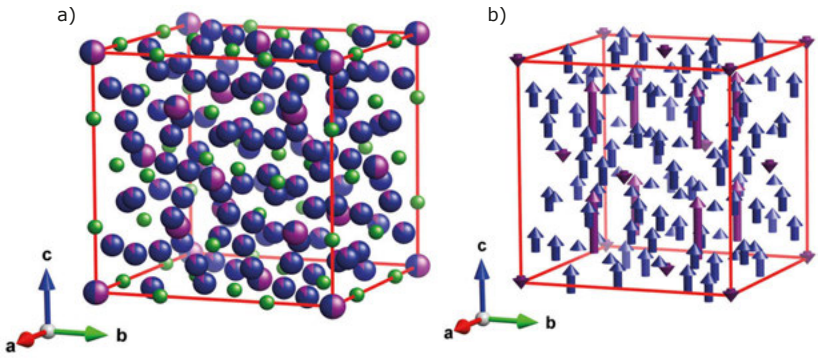

Figure 4.5. a) The structure extracted from refinements with the occupancies shown. B in green, Mn in purple and Co in blue. b) The magnetic moment at the sites for the structure. The colours denote the dominant element in the position.

4.2 Use of data-mining

Another method of finding magnetic materials was sought through the theoretical prediction of properties. Data-mining was conducted to search through libraries of materials in order to find potential compounds with good magnetic properties. Several potential systems were proposed, but the attention was turned to the most promising of these, Mn_2Co_3Ge.

4.2.1 Predicted and measured properties of Mn_2Co_3Ge

In paper III the initial prediction and synthesis was done. Previous screening attempts had been conducted using requirements of a magnetic saturation above 1 T, a Curie temperature above 400 K, a large uniaxial magnetic anisotropy energy above 1 MJ/m^3 and a magnetic hardness larger than 1. These were in addition to requirements of no oxides, rare-earth elements or AFM structures, as well as limiting the considerations to only hexagonal or tetragonal structures.

The screening done here relaxed several constraints including saturation magnetisation, which had to be larger than 0.4 T, magnetic anisotropy energy which should exceed 0.6 MJ/m^3, and only considering non-cubic systems composed of two types of 3*d*-elements. The loosening of these restrictions were motivated by a desire to find new classes of materials, where the substitution method could then be applied. The resulting systems uncovered by this search are seen in table 4.4.

Following this initial filtering of the materials, the spin structure was calculated to estimate which system was the most likely to order ferromagnetically. Mn_2Co_3Ge was the only material that seemed to be ferromagnetic, and as a

Table 4.4. *Predicted MAE, saturation magnetisation, Curie temperature and magnetic hardness parameter of the most promising materials found by the theoretical screening.*

Material	Space group	MAE (MJ/m^3)	Sat. magn. (T)	T_C (K)	κ
$ScFe_4P_2$	136	0.71	0.65	NC	1.45
Co_3Mn_2Ge	194	1.44	1.71	700	0.79
$Mn_3V_2Si_3$	193	0.85	0.73	NC	1.42
ScMnSi	189	0.69	0.52	NC	1.79
$Cu_2Fe_4S_7$	51	0.90	0.37	NC	2.87

result it was chosen for synthesis and characterisation. A reasonably pure sample was attained after synthesis, the X-ray model refinement of which can be seen in figure 4.6.

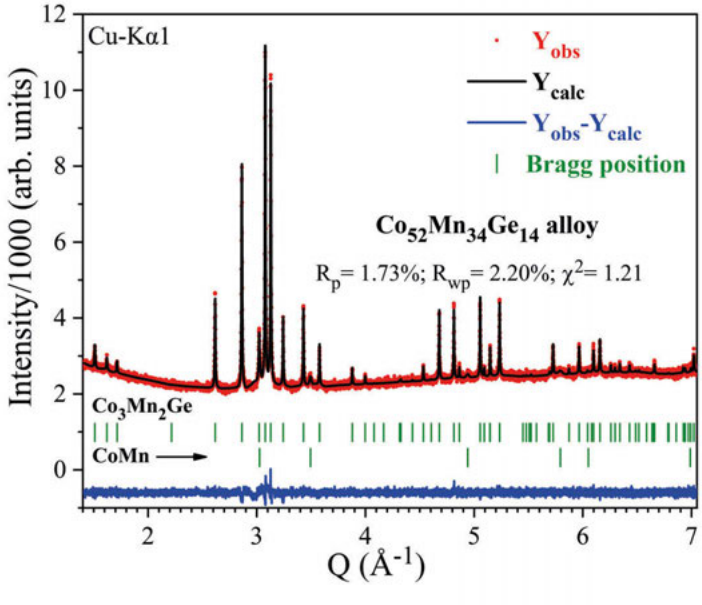

Figure 4.6. Model refinement of the powder XRD data of the $Co_{52}Mn_{34}Ge_{14}$ sample. The observed (Y_{obs}), calculated (Y_{calc}) and the difference curve (Y_{obs}-Y_{calc}) are presented along with the Bragg reflections for the two phases present.

The model refinements indicated that the structure of Mn_2Co_3Ge had a large degree of intermixing between Co and Ge on the 2*a* and 6*h* sites while Mn atoms entered exclusively into the intended 4*f* site, as this presented the best R-values. The intermixing on these particular crystallographic positions

is very common in these systems, with the exclusive occupation of the $4f$ site likewise being normal. This particular structure, however, had been reported to have both ordered and disordered structures, which can be seen in figure 4.7. The properties which had been calculated during the screening had been for the completely ordered system, as the disordered system was expected to be much less stable than the ordered one. This was based on energy calculations seen in figure 4.8, which revealed that a temperature of 2300 K was needed for the disordered system to be more stable than the ordered structure.

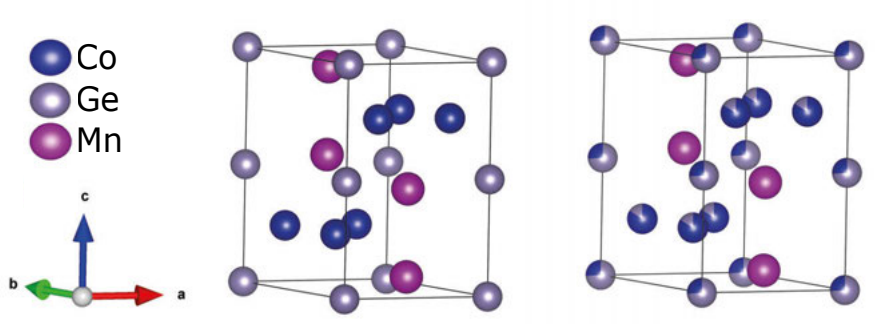

Figure 4.7. The left shows the predicted ordered Mg_2Cu_3Si-type structure of Mn_2Co_3Ge. The right shows the experimentally observed Mn_2Co_3Ge of the $MgZn_2$ structure type.

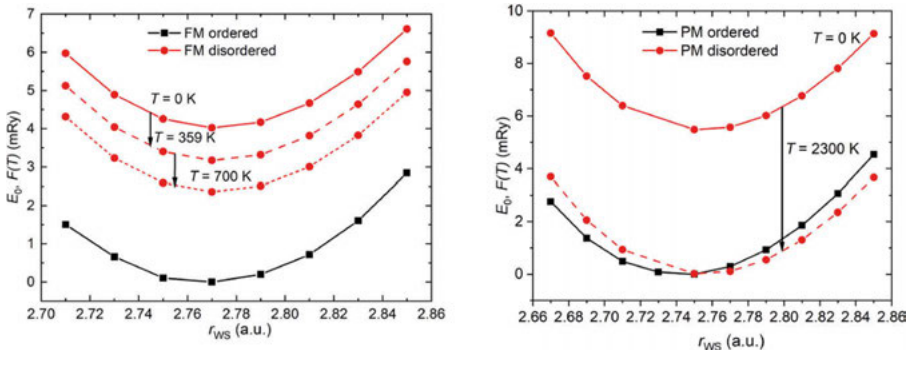

Figure 4.8. The left panel shows the normalised energies calculated for the ordered and disordered ferromagnetic structures of Mn_2Co_3Ge, at 0 K, the observed 359 K and the predicted 700 K. The right panel shows the normalised energies calculated for the paramagnetic structure, at 0 K and 2300 K, the temperature at which the disordered structure is predicted to be more stable than the ordered.

Though the magnetic properties were calculated for a completely ordered system, this intermixed system still exhibited the properties of a ferromagnet at room temperature. Nevertheless, a sizeable difference between the predicted properties was seen. The ferromagnetic structure was predicted at 0 K, but, as seen in figure 4.9 the system transforms into a non-collinear structure below

175 K. Furthermore, the Curie temperature was measured to 359 K, much lower than the predicted 700 K. The magnetic saturation also suffered, as it was measured to be 0.86 T at 10 K, which is about half of the 1.71 T predicted. The other parameters used to determine a good magnet were also impacted. The anisotropy energy experienced a small decrease, but as a result of this and the change in saturation, the hardness parameter increased. Curiously, additional calculations of the local moments of Co and Mn in the ordered and disordered structures showed similar values, indicating that something more complex was going on, and that the decrease in properties could not be ascribed solely to the intermixing.

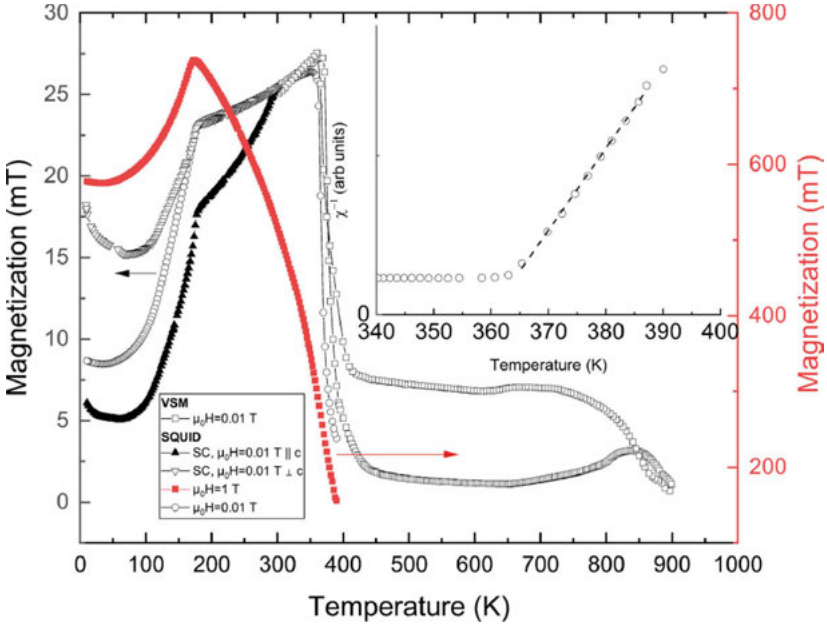

Figure 4.9. Magnetisation of the Mn_2Co_3Ge sample with respect to temperature and applied field. The white open circles and rectangles denote an applied field of 0.01 T, while the red rectangles are for an applied field of 1 T. Data for a single crystal of Mn_2Co_3Ge are also seen, with the 0.01 T field parallel (black triangles) or perpendicular (white triangles) to the crystallographic c-axis. The inset displays a Curie-Weiss fit for the inverse magnetic susceptibility revealing T_C to be 359 K.

4.2.2 The magnetic structure of Mn_2Co_3Ge

A new magnetic system was found, but several questions remained from the previous study. The ordering of the system, the appearance of non-collinear ordering, and the reason for the low magnetisation compared to what was predicted all remained unexplained. These questions were resolved in paper IV, where neutron diffraction measurements were conducted. A pure sample was

synthesised and its magnetic properties measured in order to identify the regions for neutron diffraction. The magnetic measurements are seen in figure 4.10, and show the Curie temperature of 329 K, and the onset of a transition to a non-collinear structure at 193 K. This transition to the non-collinear structure was not a sharp transition, but rather occurred over a large temperature range. This temperature range was attributed to a slow magnetic relaxation process due to domain wall movements.

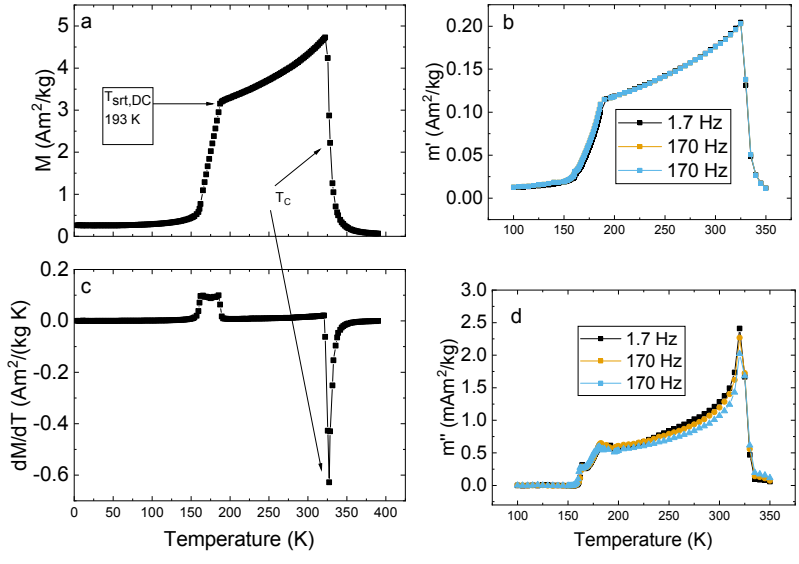

Figure 4.10. a) Magnetisation versus temperature curve under an applied field of 0.01 T, the derivative of which can be seen in c). The magnetisation using an AC excitation field of 0.4 mT with frequencies of 1.7 Hz, 17 Hz and 170 Hz are shown in b), for the in-phase component, and d) for the out-of-phase component.

The neutron diffraction patterns in the paramagnetic state revealed several reflections which could not be indexed to the $MgZn_2$-type unit cell. Instead expanding the unit cell in the a and b directions to have parameters a = 9.5932(2) Å and c = 7.7440(2) Å was necessary to describe the data. This larger structure arose due to Ge and Co showing a preference for specific crystallographic sites. Instead of the same intermixing on all the derived sites, Ge preferred the 6h derived 12j site, and the 2a site, with all other superstructure derived sites being dominated by Co. A comparison of the $MgZn_2$-type structure and the one observed can be seen in figure 4.11.

The change in the diffraction patterns due to temperature, seen in figure 4.12 was examined to establish the different magnetic structures and the individual contributions of the atoms on the sites. The initial information gleaned from the diffraction patterns showed good agreement with what had been seen with

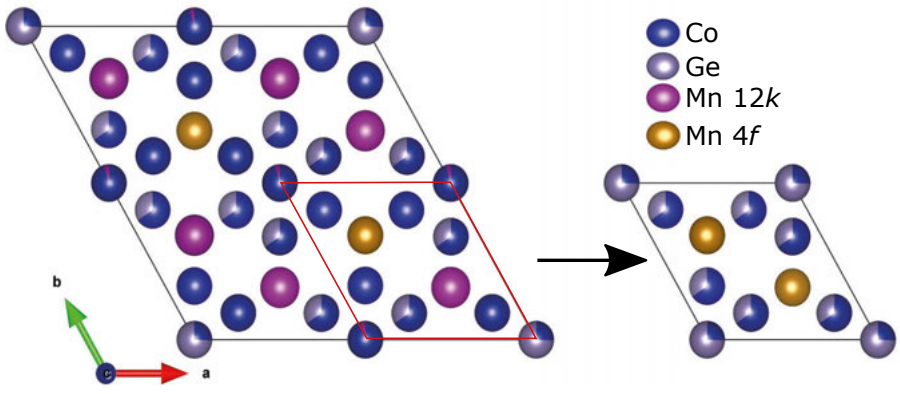

Figure 4.11. On the left the new, larger unit cell with 2 × the *ab*-direction is seen and on the right is the smaller $MgZn_2$-based unit cell.

magnetometry. Notably, that the magnetic structures consisted of a ferri- or ferromagnetic structure, and an incommensurate structure, with a transition region between the two.

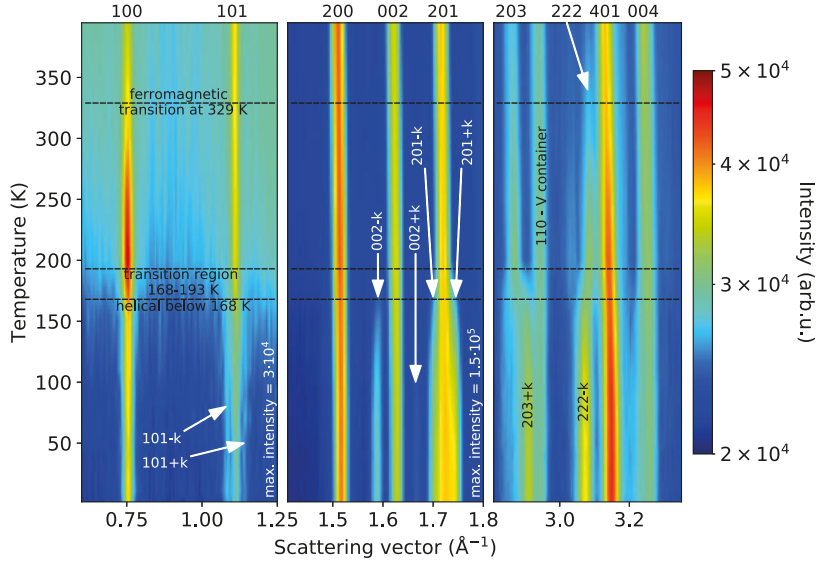

Figure 4.12. Heat map of the evolution of the diffraction peaks seen in the NPD data. The increase in intensity of certain reflections such as (100) and (222) in the ferromagnetic region, are indicative of a propagation vector **k** = (0 0 0). Additional satellites appearing around the main Bragg reflections indicate an incommensurate structure with propagation vector **k** = (0 0 0.0483).

Model refinements of the collinear structure showed that the structure was indeed that of a ferromagnet, with no anti-aligning moments. The Co atoms

had relatively similar size moments throughout the whole structure of around 0.7–1 μ_B with the variations attributed to differences in local chemical environment. The Mn moments had a much larger difference between the two main sites being 2.45(5) μ_B and 1.51(3) μ_B for the $4f$ and $12k$ site respectively. A visual comparison between the two Mn moment is seen in figure 4.13, with the surrounding moments giving an indication that the local chemical environment plays a role in stabilising the Mn moment.

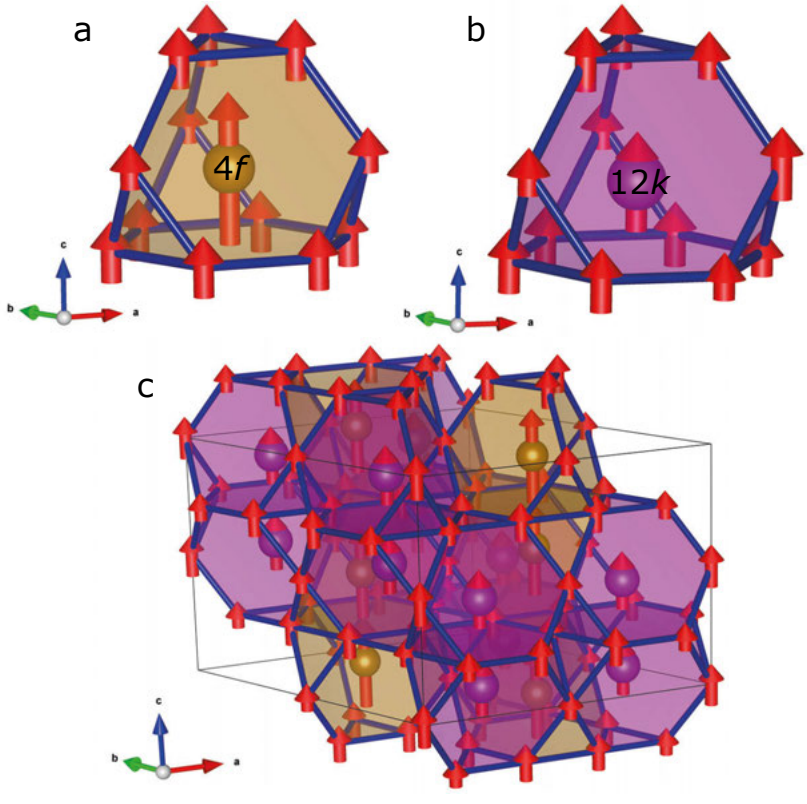

Figure 4.13. Coordination polyhedra for the $4f$ (a) and $12k$ (b) Mn atoms in the ferromagnetic phase at 200 K. The surrounding moments relate to the coordiating atoms. In c) the structure built by the two polyhedra is seen.

The incommensurate structure is depicted in figure 4.14. In this configuration the moments shift from being aligned in the *c*-direction to aligning in the *ab*-plane, and propagating helically along the *c*-direction. Here the Mn atoms split into two pairs which align with an angle close to 120° between them. This complexity hints to the intricate nature of the interactions which likely complicate calculations.

As the temperature was lowered to 1.8 K almost all magnetic moments increased in size, with the sizeable difference between the moments of the two Mn sites being maintained, as seen in table 4.5. Values extracted from

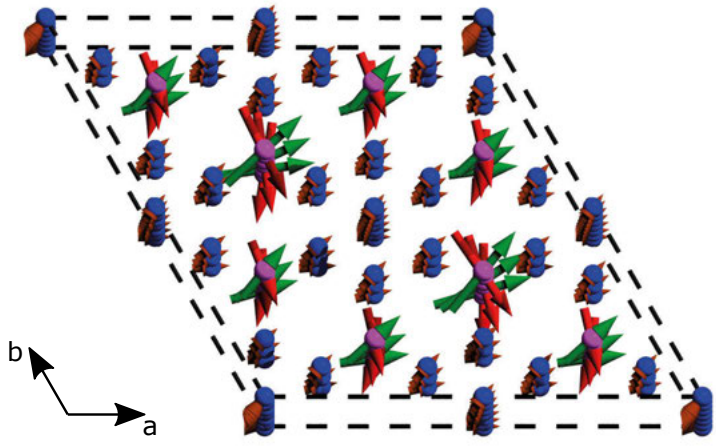

Figure 4.14. The propagation of magnetic moments in the incommensurate structure through three unit cells, seen along the c-axis. Red and green arrows are assigned to one of each of the split Mn pairs.

theoretical calculations are also presented in this table. The theoretical calculations done in the data-mining study assumed that thermal fluctuations did not impact the system much, and used 0 K for the calculations. These values did agree well with the low temperature model but differed significantly from the 200 K case. By taking into account the itinerant nature of the local moments using longitudinal spin fluctuations, good agreement was found with the ferromagnetic structure at 200 K. Furthermore, this method was also used to successfully resolve the difference in the Curie temperature, indicating that itinerant nature of the Co-atoms is the reason for the discrepancies seen.

Table 4.5. *Theoretical site resolved magnetic moments in units of μ_B for 0 K collinear ferromagnetic (FM) structure together with local element and site resolved moments at temperatures well above T_C (DLM) and for temperatures close to T_C (LSF). The moments extracted from model refinements of NPD data are also presented. The standard error is shown in the parentheses.*

Atom	Wyckoff position	FM @ 0 K	DLM @ 0 K	LSF @ 300 K	measured @ 1.8 K	measured @ 200 K
Mn1	4*f*	3.28	3.06	3.02	4.48(7)	2.45(5)
Mn2	12*k*	3.29	3.06	3.02	3.06(3)	1.51(3)
Co1	2*a*	1.70	0.68	1.05	0.63(46)	1.10(37)
Co2	6*g*	1.55	0.10	0.83	1.48(5)	0.72(5)
Co3	6*h*(1)	1.73	0.42	0.94	1.65(3)	0.98(3)
Co4	6*h*(2)	1.39	0.00	0.70	1.48(5)	0.72(3)
Co5	12*j*	1.64	0.71	0.99	1.65(3)	0.98(3)

4.2.3 Substitutions in Mn_2Co_3Ge

With a new magnetic system in hand, and an understanding of the origin of the discrepancies, improvements to the material using substitution method were attempted. Alternatives to expensive Ge had already been proposed in paper III, with especially Al and Ga being interesting candidates due to the magnetic anisotropy energy being relatively large. Synthesis of Mn_2Co_3Al was unsuccessful as the Heusler phase $MnCo_2Al$ formed instead. Synthesis of Mn_2Co_3Ga also did not succeed as it primarily formed MnCo with a small amount of Heusler. It was possible to synthesise Mn_2Co_3Si, but this material had significantly smaller magnetic moment than the Ge-based system.

Instead, attention was turned to replacing Co. This was first attempted with Mn, as a homogeneity range had previously been seen. As was discussed for the $Mn_3Co_{20}B_6$ system, the possibility that additional Mn might help stabilise the ferromagnetic state was also of interest. The anti-ferromagnetic coupling seemed to be strengthened in this system as the ferromagnetic region in temperature narrowed, and the magnetisation decreased, as seen in figure 4.15. The narrowing of the temperature region did provide a potential application within magnetocalorics, as this transition region would permit a phase transition to take place rather quickly, an essential feature for a magnetocaloric material.

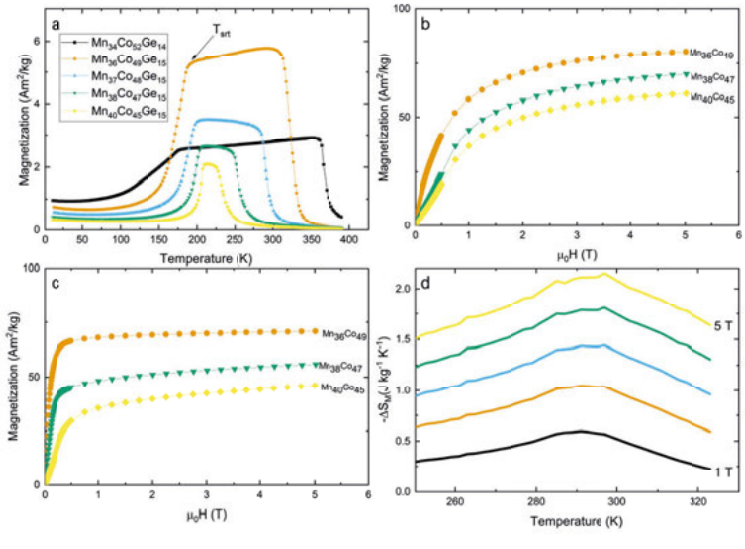

Figure 4.15. In a) the magnetisation versus temperature curves in a magnetic field of 0.01 T are shown. The magnetisation versus field curves for 2 K and 200 K are seen in b) and c) respectively. d) shows the change in isothermal magnetic entropy at different fields.

4.3 Unexpected structures

New materials have successfully been developed using the substitutional approach as well as theoretical screening. During the development of these materials, however, new stable systems were discovered. This section will cover this final method of finding new potential material systems to work with.

4.3.1 A new variant of the X-phase

During the initial synthesis attempts of Mn_2Co_3Ge an excess of Mn content was used, as this element often evaporates during alloy syntheses. It was noted that increasing amounts of Mn reduced the amount of the main competing phase, $MnCo_2Ge$. Up to 3 wt.% also increased the amount of the $MgZn_2$-type phase, and as a result larger quantities were used in the hopes of further improvements. Beyond the 3 wt.% of excess Mn however, there was little to no increase in the phase purity and at 7 wt.% excess Mn new reflections appeared which was determined to be a new phase.

The two samples of the system crystallised in the orthorhombic space group *Pnnm* with stoichiometries $Mn_{14}Co_{16.2(3)}Ge_{6.8(3)}$ and $Mn_{14.9(5)}Co_{15.5(4)}Ge_{6.6(2)}$. A large degree of ordering was observed for the various elements, with Mn, Co and Ge all having preferred sites, whilst the intermixing was contained on the high multiplicity sites of 8*h*. The interatomic distances for the atoms were between 2.33(1) and 3.01(1) Å, with the majority of the distances being between 2.60 and 2.85 Å. As Mn moments often first exhibit ferromagnetic ordering when the distances are above 2.9 Å, it was not expected to be ferromagnetic at room temperature, and no indications of this were seen.

4.3.2 New Ce based structures

In paper VII synthesis of Fe/Mn and Co/Mn based Th_2Ni_{17}-type structures, and Co/Mn and Ni/Mn based $ThMn_{12}$-type structures were attempted. Instead of producing the desired phases, however, the diffraction patterns indicated multiphase systems, or new potential structures. For the Fe/Mn based system a match with the diffraction pattern was found with the structure-type $Nd_3(Ti_{0.21}Fe_{0.79})_6Fe_{23}$, as seen in figure 4.16. This system is a member of the monoclinic space group $P2_1/c$ with unit cell parameters a = 10.5751(1) Å, b = 8.5396(1) Å, c = 9.6915(1) Å and β = 96.877(1)°. Attempts to synthesise the same structure with Co failed, as seen in figure 4.17. As all reported instances of the structure, except one, consist of Fe, it is likely that Fe along with the VEC plays a significant role in stabilising the structure.

The Co/Mn alloy adopted an ordered version of the $Ce(Ni,Mn)_{11}$ structure type, space group $P4/mbm$ with a = 8.2030(1) Å and c = 4.7152(1) Å. This structure-type was also seen for other syntheses of the system where the amount of it was determined by the Mn-content. For $CeCo_{14}Mn_3$ the alloy

mainly formed the Th_2Zn_{17}-type structure while larger amounts of Mn resulted in the formation of the $Ce(Ni,Mn)_{11}$-type structure. The Ni/Mn system crystallised in the disordered version of the $Ce(Ni,Mn)_{11}$-type structure with unit cell parameters a = 8.3667(2) Å c = 4.9225(1) Å.

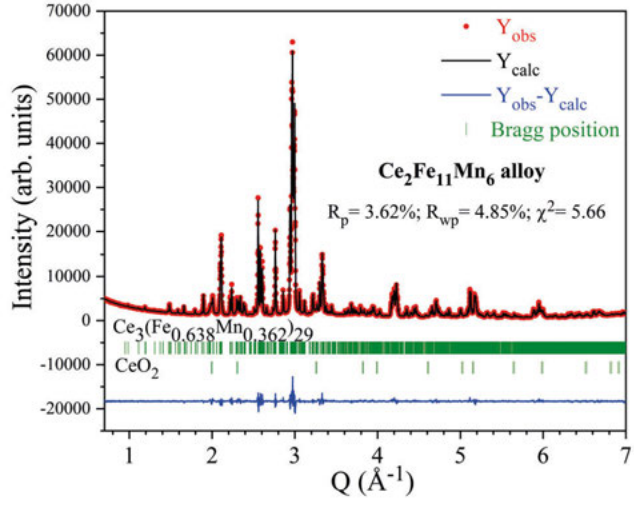

Figure 4.16. Model refinements of the XRD data for $Ce_2Fe_{11}Mn_6$.

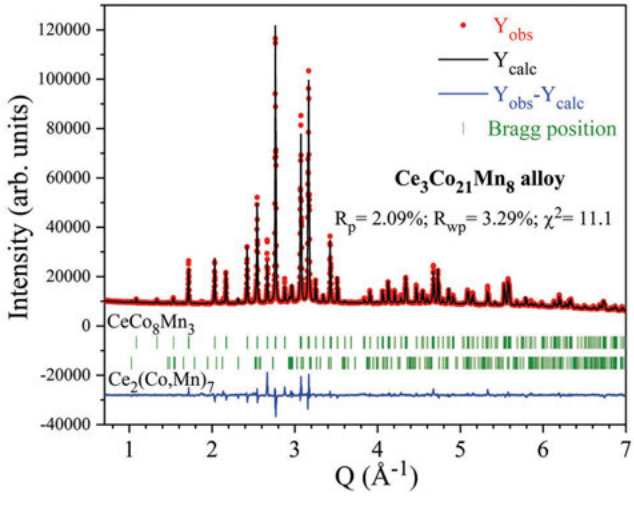

Figure 4.17. Model refinements of the XRD data for $Ce_3Co_{21}Mn_8$.

The low-field magnetisation versus temperature and field dependent magnetisation curves of the materials are presented in figure 4.18. The Fe/Mn compound showed indications of a ferrimagnetic ordering with a transition temperature above 400 K, and a magnetisation at 10 K with a 2 T applied field of 3.7 μ_B/f.u. Considering the interactions seen for Ce_2Fe_{17} and the large range of interatomic distances, this magnetic configuration is not surprising. The $Ce(Ni,Mn)_{11}$ based systems both showed indications of being canted anti-ferromagnets, which resulted in the low magnetisation seen for the systems. The Co/Mn system reached a magnetisation of 0.6 μ_B/f.u., with a transition temperature above 400 K, while the Ni/Mn system did not even reach 0.1 μ_B/f.u. and transitioned at around 300 K.

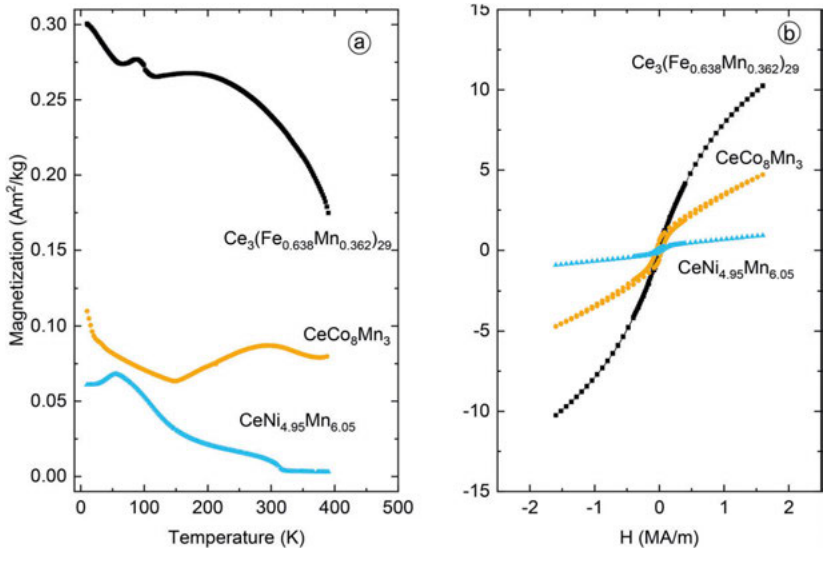

Figure 4.18. Magnetisation curves versus temperature for the Fe/Mn, Co/Mn and Ni/Mn based Ce alloys in a 0.01 T applied magnetic field are seen in a). Magnetisation versus applied field curves at a temperature of 10 K are seen in b).

5. Summary and conclusions

"And if one day she comes to you
Drink deeply from her words so wise
Take courage from her as your prize
And say hello from me"
-Uriah Heep

Several approaches to find, tune and synthesise new magnetic materials have been explored. Focussing on the crystal structure itself, several materials were synthesised based on chemical intuition using substitutional methods, directed by theoretical calculations or found by careful examination of data from assumed synthesis failures of other materials.

The substitutional method was first applied in two systems the high-entropy alloy system AlCoCrFeNi as well as the $Cr_{23}C_6$-based system $Mn_3Co_{20}B_6$. In AlCoCrFeMnNi, a random distribution of the substituting element, Mn, was attempted in increasing amounts and resulted in a significant improvement in the saturation magnetisation, but at the cost of a lower stability of the phase. While it did not exceed already established systems, such as Alnico, the inclusion of Mn, an element not used in Alnico, does show a potential avenue to increase magnetisation. In $Mn_3Co_{20}B_6$, specific sites were targeted in an attempt to control Mn distances and avoid the anti-ferromagnetic interactions. This was only partially successful as, while the targeted sites were generally occupied by Mn, a large degree of intermixing was seen. The overall magnetic structure assumed a ferrimagnetic orientation, which theoretical calculations indicated would still have occurred had the targeted substitution succeeded perfectly. In fact, the calculations indicated that some intermixing was beneficial for stabilising a ferromagnetic state.

Theoretically screened searches resulted in the material Mn_2Co_3Ge being brought to light. There were several discrepancies between the predicted and observed properties of the material. While Mn_2Co_3Ge was magnetic, the saturation magnetisation and Curie temperature were much lower than expected and the material also lost the ferromagnetic structure at lower temperatures. Another discrepancy was found in regards to the stability of the ordered and the disordered structure, where an ordered structure was expected to be much more stable than the disordered. This was resolved using neutron diffraction, which revealed a new ordered structure and complex interactions between Mn atoms. Furthermore, additional theoretical calculations indicated that temperature had a larger effect on the magnetic properties than previously expected.

The substitutional method was also applied in an attempt to reduce the amount of the more expensive materials present. Generally these were unsuccessful, though additional Mn could be used to tune the transition temperature, which could be a potential magnetocaloric material.

New systems based on magnetic elements were discovered while attempting to synthesise other materials. The new phases in the Mn-Co-Ge based system were found due to Mn excess during synthesis of Mn_2Co_3Ge, while the Ce based systems arose due to small divergences of Ce content when synthesising stoichiometric Ce_2M_{17} and CeM_{12} phases. Different elements played an important role in which structures formed, as while $Ce_3(Fe,Mn)_{29}$ was formed with Fe and Mn, Co did not form it, indicating that the VEC likely plays a large role in determining if some of these structures are formed. None of these structures showed much promise as applicable magnetic materials, but a better understanding of them could provide insight into how to tune these systems.

The substitution method, while a potent and very useful approach for tuning the properties in well-known magnetic systems, it needs to be employed with some care. In some systems, like $Mn_3Co_{20}B_6$ and AlCoCrFeMnNi, randomness with some site preferences can be achieved, and while this can lead to general trends in the properties, specific properties can be hard to control. For other systems, specific positions such as the Mn sites in Mn_2Co_3Ge can be controlled better. Unfortunately, this can also lead to restrictions in what can actually be substituted while maintaining good properties, as even exchange of the non-magnetic element in the system failed, or resulted in severely reduced the magnetic properties.

Theoretical screening can be useful to get an initial indication of the properties to expect for a system, which can provide an excellent springboard for other systems. Care must still be taken for this method, as was seen for Mn_2Co_3Ge system, which significantly overestimated in properties. Nevertheless, theoretical calculations did hint at underlying properties and ordering, which required thorough experimental investigation to observe, highlighting the potential of the approach.

Direct methods to discover new materials are risky but can nevertheless pay off if smart use of materials is considered, as has been seen with the discovery of $Nd_2Fe_{14}B$. The new structures could provide a basis for further substitutions or theoretical screening. Theoretical screening can help narrow down the materials considered and provide hints to other structures,and new structures can be passed to the theoreticians for further insight. All methods discussed here should be considered useful tools, and should be opportunistically applied by the prospective researcher.

6. Sammanfattning på svenska

"Vandraren har ingenstans att gå, när han kommit fram till slutet"
-Nordman

Magneter spelar en viktig roll i dagens samhälle, där de används vid till exempel energiproduktion, energiomvandling och datalagring. Det finns dock relativt få typer av magnetiska material som används till dessa viktiga uppgifter. Orsaken till detta är att det är väldigt svårt att hitta material som har de nödvändiga egenskaperna för de applikationerna. Det är många parametrar som avgör hur bra ett magnetiskt material är, till exempel magnetisering, och den temperatur vid vilken materialet ordnar sig ferromagnetiskt, också kallat Curietemperaturen. Dessa parametrar påverkas av vilka grundämnen som materialet består av, vilken kristallstruktur det har och dess mikrostruktur. I den här avhandlingen undersöks olika sätt att hitta nya magnetiska material genom att ändra på grundämnen, och söka nya kristallstrukturer. Den första av metoderna är substitutionsmetoden, där några atomer i specifika strukturer blev utbytta mot ett annat grundämne. Detta är en vanlig metod att ändra på egenskaperna av ett material, till exempel i stål, där styrkan kan ökats beroende på vilka grundämne som substitueras in. Nyligen har datautvinning eller ”data-mining” börjat bli en ny metod att hitta nya strukturer. Genomsökning av en databas och uppskattning av egenskaper utifrån teoretiska metoder kan några strukturer föreslås som potentiella användbara material.

Först undersöktes substitutionsmetoden, där några atomer i specifika strukturer blev utbytta mot ett annat grundämne. I $AlCoCrFeMn_xNi$ blev mangan introducerat i strukturen. Mangan är inte magnetiskt själv då interaktioner mellan manganatomerna inte tillåter ferromagnetisk ordning, men när dessa interaktionerna undviks har den potential att uppvisa större magnetisering än järn. Detta observerades också i $AlCoCrFeMn_xNi$ där magnetiseringen ökade med ökande mängd mangan, dock blev systemet mer instabilt och Curietemperaturen blev lägre. I $Mn_3Co_{20}B_6$ gjordes försök att introducera mangan på specifika positioner. Detta undersöktes med neutrondiffraktion, där resultaten påvisade att det delvis lyckades. Mangan föredrog de två positioner i strukturen de avsågs för, men fanns även på andra positioner i systemet. Mangan bidrog med det högsta magnetiska momentet i systemet, relativt till mängden. Den magnetiska strukturen var ferrimagnetisk, och teoretiska beräkningar visade att även om mangan bara hade varit på de avsedda positionerna hade den ferrimagnetiska ordningen bestått. Beräkningarna antydde också att mangan på andra positioner faktisk stabiliserade en ferromagnetisk struktur, och en

kontrollerad blanding på positionerna skulle kunna vara gynsam för de magnetiska egenskaperna. Substitioner av mangan kan därför vara ett bra sätt att öka magnetiseringen, dock med risk för minskande termisk stabilitet.

Efter screening av många material genom undersökningar med teoretiska beräkningar hittades Mn_2Co_3Ge som en möjlig kandidat för magnetiska applikationer. Tyvärr var både magnetiseringen och Curietemperaturen lägre än väntat och alltså inte lika optimistiska som beräkningarna antydde. Orsaken till detta antogs ursprungligen vara att Co och Ge inte blev perfekt ordnat som väntat från beräkningarna. Det undersökta provet visade sig ha en annan struktur, med större dimensioner, än den teoretiska. Det berodde på en skillnad i ordningen av Co och Ge. I den magnetiska strukturen hade alla Co atomerna liknande magnetisering, medan magnetiseringen för Mn varierade beroende på dess omgivning i kristallstrukturen. Nya beräkningar gjordes där temperaturfluktuationer tilläts, och det passade bra för alla Co atomerna. Vid lägre temperatur blev den ferromagnetiska strukturen omvandlad till en helixstruktur med väldig komplicerade interaktioner mellan Mn atomerna. Vid den lägsta temperaturen där termiska fluktuationer nästan inte existerar, sågs en bra överensstämmelse med de ursprungliga beräkningarna, även om strukturen inte var ferromagnetisk vid den temperaturen. Systemet var alltså mer känsligt för temperaturpåverkan än väntat och detta påverkade beräkningarna. Då Mn-halten i materialet ökas, sänks Curietemperaturen, och skulle då kunna användas som ett magnetokaloriskt material, ett material som kan används till magnetisk kylning. Mn_2Co_3Ge är ett interessant nytt material som har potential att användas till, inte bara magnetisk kylning, utan även ett modellsystem för att förstå mangans kemi och magnetism. En god förståelse av Mn krävs för att ge bra föreslag till teoretiska beräkningar för system med Mn. En god förståelse kan också göra det lättare att veta vilka system det kan finnas nya användningar till.

Nya material blev också upptäckta vid syntesförsök av andra strukturer. Försök att syntetisera Mn_2Co_3Ge resulterade i materialen $Mn_{14}Co_{16.2}Ge_{6.8}$ och $Mn_{14.9}Co_{15.5}Ge_{6.6}$. Dessa har en sällsynt struktur som bara har observerats i två andra fall. Tyvärr var dessa inte magnetiska, vilket nog berodde på den stora mängd av mangan med litet avstånd dem emellan. Några Ce-baserad strukturer hittades under syntesförsök av två andra strukturtyper med Ce:metall i förhållande 1:12 eller 2:17. I järn/mangan systemet var det istället strukturen $Ce_3(Fe_{0.638},Mn_{0.362})_{29}$ som sågs. Det var en kombination av 1:12 och 2:17 systemen och hade tecken på ferrimagnetisk struktur med en hög Curietemperatur. Då dess magnetisering var låg, är den inte användbar i nuläget. Kombinationer av substitutionsmetoden och beräkningsmetoder kan möjligen förbättra egenskaper och göra materialet intressant i framtiden. Flera andra system med Ce undersöktes och intressanta strukturer erhölls. Dock var de magnetiska egenskaperna för dåliga för användning i potentiella applikationer. Dessa nya system kan dock bli intressanta att undersöka med teoretiska beräkningar för att hitta andra nya magnetiska material med bättre egenskaper.

Sammanfattningsvis så har olika sätt att hitta nya magneter studerats. Både substitutioner i kända stukturer och material hittade med teoretiska metoder resulterade i intressanta resultat. Huvudbudskapet från detta är att man alla metoderna borde användas sammantaget, då de fungerar bäst tillsammans.

7. Acknowledgements

"I know I have friends,
I am never alone,
but I am a wanderer,
the road is my home"
-Wuthering Heights

To my supervisors, Martin, Johan and Paul, thank you for giving me this opportunity to learn and grow. I hope that I have not been too much of a burden throughout the years and that I have lived up to your expectations. It has been fantastic to be introduced to the field of magnetic materials and being able to collaborate on such wide level. I would do it all again if I could.

To my collaborators from Solid State Physics, Daniel, Henry and Peter, as well as Sagar, thank you for all the help throughout the years, I hope my spontaneous visits to discuss ideas and questions have not been too annoying. My collaborative friends from the Physics department, Erna, Alena, Rafael, Heike and Olle, I would like to thank for the wonderful work done. I would also like to apologise for the discoveries we made making your calculations more difficult, but such is reality. Thank you for taking it in strides! Vitalii, thank you for the immense help with synthesis as well as all the advice provided. Your ability to make something from mistakes is inspiring, and what we have made from my mistakes has been great! I hope we get to collaborate again in the future. Rebecca, thank you for being a driving force for the afterwork pub visits. I doubt that I would do much of it myself were it not for you. Perhaps in the future we will have a chance to work together more! The basement crew of Gustav, Dennis, Victor, Ocean, Julia, Amanda, Irene and Ivan also deserve thanks for making the basement a fun place to work! A big thank you Pedro for keeping the lab as nice as it is, and for your advice during the desperation synthesis. Mikael O. as well, for keeping the diffraction lab working. I also wish to thank Premek for sharing of his immense knowledge of magnetic structures.

To my office mates Adriano and Mikael A. thank you both for your positive attitude, encouraging words for when I have been doubting myself, and the many fun discussions throughout the years. I will miss having such fantastic office partners.

To all people of Inorganic and Structural Chemistry thank you for being you, and providing the fantastic social environment that I have enjoyed the past many years. Barbara, Tatiana, Max and Chris, a special thank you for

making me feel welcome during the first couple of weeks here in Uppsala. Isabell and Simon, my namebrother, thank you for arranging so many fun events, I hope we get to do it even after our time here! Will and Veronica, thank you for gin and tonic and game nights and the many discussions about life. Robin thank you for always being such a positive person to be around. To the Dungeons and Dragons group of Isabell, Simon, Robin, Chris, Adriano, Jorge, Rebecca and Will, thank you for the many late nights full of crazy fun to distract from all the stress of reality.

To my family and all my other friends throughout the years, thank you for your support and keeping me somewhat sane during these last tumultuous years.

References

[1] J. Keithley, *The story of electrical and magnetic measurements: from 500 B.C. to the 1940s*. New York: IEEE Press, 1999.

[2] J. Livingston, "The history of permanent-magnet materials," *JOM*, vol. 42, pp. 30–34, 1990.

[3] J. Coey, *Magnetism and Magnetic Materials*. Cambridge: Cambridge University Press, 2010.

[4] O. Gutfleisch, M. Willard, E. Brück, C. Chen, S. Sankar, and J. Liu, "Magnetic materials and devices for the 21st century: Stronger, lighter and more energy efficient," *Advanced Materials*, vol. 23, pp. 821–842, 2011.

[5] J. Coey, "Permanent magnets: Plugging the gap," *Scripta Materialia*, vol. 67, pp. 524–529, 2012.

[6] L. Patrick, "Antiferromagnetism of manganese," *Physical Review*, vol. 93, p. 370, 1954.

[7] J. Slater, "Atomic shielding constants," *Physical Review*, vol. 36, pp. 57–64, 1930.

[8] C. Zener, "Interaction between the *d* shells in the transition metals," *Physical Review*, vol. 81, pp. 440–444, 1951.

[9] E. Morgan, "Ferromagnetism of certain manganese-rich alloys," *Journal of Metals*, vol. 6, pp. 983–988, 1954.

[10] J. Coey, "New permanent magnets; manganese compounds," *Journal of Physics and Condensed Matter*, vol. 26, p. 064211, 2014.

[11] H. Kono, "On the ferromagnetic phase in manganese-aluminum system," *Journal of the Physical Society of Japan*, vol. 13, pp. 1444–1451, 1958.

[12] A. Koch, P. Hokkeling, M. Steeg, and J. de Vos, "New material for permanent magnets on a base of Mn and Al," *Journal of Applied Physics*, vol. 31, p. S75, 1960.

[13] J. Yeh, S. Chen, S. Lin, J. Gan, T. Chin, T. Shun, C. Tsau, and S. Chang, "Nanostructured high-entropy alloys with multiple principal elements: Novel alloy design concepts and outcomes," *Advanced Engineering Materials*, vol. 6, pp. 299–303, 2004.

[14] B.Cantor, I.T.H.Chang, P.Knight, and A.J.B.Vincent, "Microstructural development in equiatomic multicomponent alloys," *Materials Science and Engineering: A*, vol. 375-377, pp. 213–218, 2004.

[15] P. Huang, J. Yeh, T. Shun, and S. Chen, "Multi-principal-element alloys with improved oxidation and wear resistance for thermal spray coating," *Advanced Engineering Materials*, vol. 6, pp. 74–78, 2004.

[16] Y. Brif, M. Thomas, and I. Todd, "The use of high-entropy alloys in additive manufacturing," *Scripta Materialia*, vol. 99, pp. 93–96, 2015.

[17] M. Sahlberg, D. Karlsson, C. Zlotea, and U. Jansson, "Superior hydrogen storage in high entropy alloys," *Scientific Reports*, vol. 6, p. 36770, 2016.

[18] P. Xie, Y. Yao, Z. Huang, Z. Liu, J. Zhang, T. Li, G. Wang, R. Shahbazian-Yassar, L. Hu, and C. Wang, "Highly efficient decomposition of ammonia using high-entropy alloy catalysts," *Nature Communications*, vol. 10, p. 4011, 2019.

[19] J. Law, L. M. Moreno-Ramírez, . Díaz-García, A. Martín-Cid, S. Kobayashi, S. Kawaguchi, T. Nakamura, and V. Franco, "MnFeNiGeSi high-entropy alloy with large magnetocaloric effect," *Journal of Alloys and Compounds*, vol. 855, p. 157424, 2021.

[20] R. Nutor, Q.P.Cao, X.D.Wang, D. Zhang, and J. Jiang, "Tunability of the mechanical properties of $(Fe_{50}Mn_{27}Ni_{10}Cr_{13})_{100-x}Mo_x$ high-entropy alloys via secondary phase control," *Journal of Materials Science & Technology*, vol. 73, pp. 210–217, 2021.

[21] B. Gwalani, S. Gorsse, D. Choudhuri, Y. Zheng, R. Mishra, and R. Banerjee, "Tensile yield strength of a single bulk $Al_{0.3}$CoCrFeNi high entropy alloy can be tuned from 160 mpa to 1800 mpa," *Scripta Materialia*, vol. 162, pp. 18–23, 2019.

[22] J.-W. Yeh, "Recent progress in high entropy alloys," *Annales de Chimie - Science des Matériaux*, vol. 31, pp. 633–648, 2006.

[23] D. Miracle and O. Senkov, "A critical review of high entropy alloys and related concepts," *Acta Materialia*, vol. 122, pp. 448–511, 2017.

[24] Y. Zhang, Y. Zhou, J. Lin, G. Chen, and P. Liaw, "Solid-solution phase formation rules for multi-component alloys," *Advanced Engineering Materials*, vol. 10, pp. 534–538, 2008.

[25] X. Yang and Y. Zhang, "Prediction of high-entropy stabilized solid-solution in multi-component alloys," *Materials Chemistry and Physics*, vol. 132, pp. 233–238, 2012.

[26] S. Guo, C. Ng, and C. Liu, "Effect of valence electron concentration on stability of fcc or bcc phase in high entropy alloys," *Journal of Applied Physics*, vol. 109, p. 103505, 2011.

[27] W.-R. Wang, W.-L. Wang, and J.-W. Yeh, "Phases, microstructure and mechanical properties of Al_xCoCrFeNi high-entropy alloys at elevated temperatures," *Journal of Alloys and Compounds*, vol. 589, pp. 143–152, 2014.

[28] S. Huang, W. Li, X. Li, S. Schönecker, L. Bergqvist, E. Holmström, L. Varga, and L. Vitos, "Mechanism of magnetic transition in FeCrCoNi-based high entropy alloys," *Materials & Design*, vol. 103, pp. 71–74, 2016.

[29] T. Zuo, M. Gao, L. Ouyang, X. Yang, Y. Cheng, R. Feng, S. Chen, P. Liaw, J. Hawk, and Y. Zhang, "Tailoring magnetic behaviour of CoFeMnNiX (X = Al, Cr, Ga and Sn) high-entropy alloys by metal doping," *Acta Materialia*, vol. 130, pp. 10–18, 2017.

[30] A. Westgren, "Complex chromium and iron carbides," *Nature*, vol. 132, pp. 480–480, 1933.

[31] X. X. Wei, W. Xu, J. L. Kang, M. Ferry, and J. F. Li, "Metastable $Co_{23}B_6$ phase solidified from deeply undercooled $Co_{79.3}B_{20.7}$ alloy melt," *Journal of Materials Science*, vol. 51, pp. 6436–6443, 2016.

[32] D. Kotzott, M. Ade, and H. Hillebrecht, "Single crystal studies on Co-containing τ-borides $Co_{23-x}M_xB_6$ (M = Al, Ga, Sn, Ti, V, Ir) and the boron-rich τ-boride $Co_{12.3}Ir_{8.9}B_{10.5}$," *Journal of Solid State Chemistry*,

vol. 182, pp. 538 – 546, 2009.
[33] Y. Kuz'ma, Y. Voroshilov, and E. Cherkashin, "New ternary compounds with $W_2Cr_{21}C_6$-type structure," *Inorganic Materials*, vol. 1, pp. 1017–1019, 1965.
[34] H. Stadelmaier, R. Draughn, and G. Hofer, "Die struktur der ternaeren boride vom chromkarbid-($Cr_{23}C_6$)typ," *Zeitschrift fuer Metallkunde*, vol. 54, pp. 640–644, 1963.
[35] H. Hirota, "Magnetic Properties of Borides with a $Cr_{23}C_6$ Structure," *Journal of the Physical Society of Japan*, vol. 23, pp. 512–516, 1967.
[36] J. Cedervall, P. Beran, M. Vennström, T. Danielsson, S. Ronneteg, V. Höglin, D. Lindell, O. Eriksson, G. André, Y. Andersson, P. Nordblad, and M. Sahlberg, "Low temperature magneto-structural transitions in $Mn_3Ni_{20}P_6$," *Journal of Solid State Chemistry*, vol. 237, pp. 343 – 348, 2016.
[37] T. Eriksson, M. Vennström, S. Ronneteg, Y. Andersson, and P. Nordblad, "Complex magnetic properties of $Mn_3Ni_{20}P_6$ and ferromagnetic structure of the new isostructural compound $Mn_3Pd_{20}P_6$," *Journal of Magnetism and Magnetic Materials*, vol. 308, pp. 203 – 209, 2007.
[38] Y. Kuz'ma and E. Gladyshevskii, "Crystal structure of the compound Mn2Co3Ge," *Dopovidi Akademii Nauk Ukrains'koi RSR*, vol. 2, p. 205, 1963.
[39] D. Thoma and J. Perepezko, "A geometric analysis of solubility ranges in laves phases," *Journal of Alloys and Compounds*, vol. 224, pp. 330–341, 1995.
[40] F. Stein, "Consequences of crystal structure differences between C14, C15 and C36 laves phase polytypes for their coexistence in transition-metal-based systems," *MRS Online Proceedings Library*, vol. 1295, pp. 299–310, 2011.
[41] V. Skripnyuk and M. Ron, "Hydrogen desorption kinetics in intermetallic compounds C2, $C5_1$ and $C5_2$ with Laves phase structure," *International Journal of Hydrogen Energy*, vol. 28, pp. 303–309, 2003.
[42] A. Halstead and R. Rawlings, "The fracture behaviour of two Co-Mo-Cr-Si wear resistant alloys ("Tribaloys")," *Journal of Materials Science*, vol. 20, pp. 1248–1256, 1985.
[43] M. Gemmill, H. Hughes, and J. Murray, "Study of 7% and 8% chromium creep-resisting steels for use in steam power plant," *Journal of Iron and Steel Institute*, vol. 184, pp. 122–144, 1956.
[44] F. Stein and A. Leineweber, "Laves phases: a review of their functional and structural applications and an improved fundamental understanding of stability and properties," *Journal of Materials Science*, vol. 56, pp. 5321–5427, 2020.
[45] J. Friauf, "The crystal structure of magnesium di-zincide," *Physical Review*, vol. 29, pp. 34–40, 1927.
[46] H. Witte, "Untersuchungen im system magnesium-kupfer-silicium mit besonderer berueecksichtigung des schnittes MgCu2–MgSi2," *Metallwirtschaft Metallwissenschaft Metalltechnik*, vol. 18, pp. 459–463, 1939.
[47] J. Florio, R. Rundle, and A. Snow, "Compounds of thorium with transition metals. i. the thorium-manganese system," *Acta Crystallographica*, vol. 5, pp. 449–457, 1952.
[48] G. Hadjipanayis, A. Gabay, A. Schönhöbel, A. Martín-Cid, J. Barandiaran, and D. Niarchos, "$ThMn_{12}$-type alloys for permanent magnets," *Engineering*, vol. 6, pp. 141–147, 2020.

[49] Y.-C. Yang, H. Sun, and L.-S. Kong, "Neutron diffraction study of $Y(Ti,Fe)_{12}$," *Journal of Applied Physics*, vol. 64, pp. 5968–5970, 1988.
[50] B.-P. Hu, H.-S. Li, and J. Coey, "Relationship between $ThMn_{12}$ and Th_2Ni_{17} structure types in the $YFe_{11-x}Ti_x$ alloy series," *Journal of Applied Physics*, vol. 67, pp. 4838–4840, 1990.
[51] J. Florio, N. Baenziger, and R. Rundle, "Compounds of thorium with transition metals. ii. systems with iron, cobalt and nickel," *Acta Crystallographica*, vol. 9, pp. 367–372, 1956.
[52] Y. Khan, "The crystal structures of R_2Co_{17} intermetallic compounds," *Acta Crystallographica*, vol. B29, pp. 2502–2507, 1973.
[53] Y. Scherbakova, G. Ivanova, N. Mushnikov, and I. Gervasieva, "Magnetic properties of $Sm_2(Fe,Ti)_{17}$ compounds and their nitrides with Zn_2Th_{17} and Th_2Ni_{17} structures," *Journal of Alloys and Compounds*, vol. 308, pp. 15–20, 2000.
[54] J. Cadogan, H.-S. Li, A. Margarian, J. Dunlop, D. Ryan, S. Collocott, and R. Davis, "New rare-earth intermetallic phases $R3(Fe,Mn)_{29}X_n$:(R=Ce,Pr,Nd,Sm,Gd; M=Ti,V,Cr,Mn; and X=H,N,C)," *Journal of Applied Physics*, vol. 76, pp. 6138–6143, 1994.
[55] O. Kalogirou, V. Psycharis, L. Saettas, and D. Niarchos, "Existence range, structural and magnetic properties $Nd_3Fe_{27.5}Ti_{1.5-y}Mo_y$ and $Nd_3Fe_{27.5}Ti_{1.5-y}Mo_yN_x$ ($0.0 \leq y \leq 1.5$)," *Journal of Magnetism and Magnetic Materials*, vol. 146, pp. 335–345, 1995.
[56] Y. Kalychak, L. Akselrud, Y. Yarmolyuk, O. Bodak, and E. Gladyshevskii, "The crystal structure of the compounds $Ce(Mn_{0.55}Ni_{0.45})_{11}$ and $U(Ni_{0.68}Si_{0.32})_{11}$," *Soviet Physics Crystallography*, vol. 20, pp. 639–640, 1976.
[57] Y. Kalychak, L. Akselrud, V. Zaremba, and V. Baranyak, "The crystal structure of the RNi_9In_2 (R= Y, La, Ce, Pr, Nd, Sm, Eu, Gd, Tb, Dy, Ho, Er) compounds," *Dopovidi Akademii Nauk Ukrains'koi RSR (Ser. B)*, vol. 8, pp. 35–37, 1984.
[58] J. Cui, J. Ormerod, D. Parker, R. Ott, A. Palasyuk, S. Mccall, M. Paranthaman, M. Kesler, M. McGuire, I. Nlebedim, C. Pan, and T. Lograsso, "Manufacturing porcesses for permanent magnets: Part i - sintering and casting," *JOM*, vol. 74, pp. 1279–1295, 2022.
[59] V. Pecharsky and P. Zavalij, *Fundamentals of Powder Diffraction and Structural Characterization of Materials*. Boston: Kluwer Academic Publishers, 2003.
[60] H. M. Rietveld, "A profile refinement method for nuclear and magnetic structures," *Journal of Applied Crystallography*, vol. 2, pp. 65–71, 1969.
[61] J. Rodríguez-Carvajal, "Recent advances in magnetic structure determination by neutron powder diffraction," *Physica B: Condensed Matter*, vol. 192, pp. 55–69, 1993.
[62] T. Jensen, T. Nielsen, Y. Filinchuk, J.-E. Jørgensen, Y. Cerenius, E. Gray, and C. Webb, "Versatile in situ powder x-ray diffraction cells for solid-gas investigations," *Journal of Applied Crystallography*, vol. 43, pp. 1456–1463, 2010.
[63] K. Yager, "Neutron scattering lengths." `http://gisaxs.com/index.php/Neutron_scattering_lengths`, 2014. (Accessed: 07-04-2021).

[64] P. Hohenberg and W. Kohn, "Inhomogeneous electron gas," *Physical Review*, vol. 136, pp. B864–B871, 1964.
[65] W. Kohn and L. Sham, "Self-consistent equations including exchange and correlation effects," *Physical Review*, vol. 140, pp. A1133–A1138, 1965.
[66] H. Ebert, D. Ködderitzsch, and J. Minár, "Calculating condensed matter properties using the KKR-Green's function method–recent developments and applications," *Reports on Progress in Physics*, vol. 74, p. 096501, 2011.
[67] J. Wills and B. Cooper, "Synthesis of band and model hamiltonian theory for hybridizing cerium systems," *Physical Review B*, vol. 36, pp. 3809–3823, 1987.
[68] J. Wills, M. Alouani, P. Andersson, A. Delin, O. Eriksson, and O. Grechnyev, *Full-Potential Electronic Structure Method*. Berlin: Springer, 2010.

Acta Universitatis Upsaliensis

Digital Comprehensive Summaries of Uppsala Dissertations from the Faculty of Science and Technology 2198

Editor: The Dean of the Faculty of Science and Technology

A doctoral dissertation from the Faculty of Science and Technology, Uppsala University, is usually a summary of a number of papers. A few copies of the complete dissertation are kept at major Swedish research libraries, while the summary alone is distributed internationally through the series Digital Comprehensive Summaries of Uppsala Dissertations from the Faculty of Science and Technology. (Prior to January, 2005, the series was published under the title "Comprehensive Summaries of Uppsala Dissertations from the Faculty of Science and Technology".)

Distribution: publications.uu.se
urn:nbn:se:uu:diva-486285

ACTA
UNIVERSITATIS
UPSALIENSIS
UPPSALA
2022